frontiers in Earth Science

ORIGINAL RESEARCH
published: 15 November 2019
doi: 10.3389/feart.2019.00298

Fluvial and Eolian Sediment Mixing During Changing Climate Conditions Recorded in Holocene Andean Foreland Deposits From Argentina (31–33°S)

Tomas N. Capaldi[1], Sarah W. M. George[1], Jaime A. Hirtz[1], Brian K. Horton[1,2] and Daniel F. Stockli[1]*

[1] *Department of Geological Sciences, Jackson School of Geosciences, The University of Texas at Austin, Austin, TX, United States,* [2] *Institute for Geophysics, Jackson School of Geosciences, The University of Texas at Austin, Austin, TX, United States*

OPEN ACCESS

Edited by:
Julie Fosdick, University of Connecticut, United States

Reviewed by:
Kurt Eric Sundell, The University of Arizona, United States
Pedro Val, Universidade Federal de Ouro Preto, Brazil

****Correspondence:***
Tomas N. Capaldi
tcapaldi@utexas.edu

Specialty section:
This article was submitted to Sedimentology, Stratigraphy and Diagenesis, a section of the journal Frontiers in Earth Science

Received: *16 August 2019*
Accepted: *29 October 2019*
Published: *15 November 2019*

Citation:
Capaldi TN, George SWM, Hirtz JA, Horton BK and Stockli DF (2019) Fluvial and Eolian Sediment Mixing During Changing Climate Conditions Recorded in Holocene Andean Foreland Deposits From Argentina (31–33°S). Front. Earth Sci. 7:298. doi: 10.3389/feart.2019.00298

Continental drainage systems archive complex records of rock uplift, source area relief, precipitation, glaciation, and carbon cyclicity driven largely by tectonics and climate. Significant progress has been made in linking such external environmental forcings to the geomorphic expression of landscapes and the stratigraphic record of depositional basins in coastal and offshore areas. However, there are large uncertainties in the degree to which sediment dispersal processes can modify signals between the erosional sources and the depositional sinks. We investigate a Holocene sediment transfer zone with contrasting fluvial and eolian sediment transport mechanisms to understand how river and wind processes impact the propagation of environmental signals in continental-scale drainage systems. To quantify these processes, we employ sediment fingerprinting methods for unconsolidated sand samples (detrital zircon U-Pb geochronology), incorporate sediment mixing models, and correlate the findings with the regional geologic and geomorphic framework. Three contrasting source regions deliver sediment to the Andean foreland: volcanic rocks of the Frontal Cordillera, sedimentary rocks of the Precordillera, and metamorphic basement of the Sierras Pampeanas. Although all samples of Holocene eolian dunes accurately record sediment input from three fluvial source regions, spatial variations in U-Pb results are consistent with north-directed paleowinds, whereby river sediments from Frontal Cordillera sources are transported northward and progressively mixed with river sediments from Precordillera and Sierras Pampeanas sources. In contrast, samples of modern rivers show progressive southward (downstream) mixing along a large axial fluvial system. Sediment mixing induced by eolian transport and reworking of various sources is likely a critical, climate-modulated process in the propagation of environmental signals, potentially involving the aliasing of tectonic signals, local storage and recycling of synorogenic river sediment, and cyclical patterns of sediment starvation and delivery to distal zones of accumulation.

Keywords: detrital zircon, Quaternary, eolian transport, fluvial megafan, modern river sediments, source to sink, Andes, Argentina

INTRODUCTION

Sediment routing systems link erosional landscapes to depositional basins and are fundamental in the transmission of surface processes, lithospheric dynamics, regional tectonics, and climate cycles to the stratigraphic record. These systems are characterized by three domains with associated sedimentary processes: (1) sediment source regions marked by relatively high-relief areas of enhanced erosion, (2) sediment transfer zones that show lower relief and generally exhibit limited erosion or accumulation, and (3) sedimentary sinks that record net sediment accumulation (**Figure 1**). Sediment routing systems respond to variations in rock uplift and source area relief (driven largely by *tectonics*), precipitation and glaciation (driven largely by *climate*), the areal extent of river drainage networks, sediment source lithology, and subsidence. Such changes in *environmental signals* are manifest as perturbations in sediment production, dispersal, and/or deposition (Romans et al., 2016). Significant progress has been made in linking environmental signals to the geomorphic expression of landscapes (Jackson et al., 2019; Sharman et al., 2019), and the stratigraphic response within the ultimate basin sink (Blum et al., 2018). However, uncertainties remain regarding the degree to which eolian transfer zones redistribute sediment and modify signals from the erosional source region to a sedimentary basin. Transfer zones are capable of altering or completely removing environmental signals through temporary non-marine sediment storage and weathering (Johnsson et al., 1988, 1991; DeCelles and Hertel, 1989), transport and mechanical breakdown (Ingersoll et al., 1993; Garzanti et al., 2015), climatic fluctuations (Castelltort and Van Den Driessche, 2003; Lawton and Buck, 2006; Mason et al., 2017, 2019; Fildani et al., 2018), autogenic processes (Jerolmack and Paola, 2010), and along-shore drift sediment mixing (Sickmann et al., 2016).

Arid to semiarid regions susceptible to the interplay of fluvial and eolian forces account for ∼17.5% of global land area (Williams and Balling, 1996; Bullard and McTainsh, 2003; Belnap et al., 2011), with sand dunes between 30°N and 30°S currently comprising 10% of the land area, which decreased from 50% during the late Pleistocene (Mehl et al., 2018). Quaternary eolian environments are primarily found in distal foreland basins of Cordilleran (e.g., Andes and North America) and collisional systems (e.g., Zagros and Himalaya), cratonic settings (e.g., Australia and Africa) (Al-Masrahy and Mountney, 2015), and comparable Martian environments (Kocurek and Ewing, 2012). Cratonic eolian systems are long-term recorders of aridification where wind reworks sediment in internally and externally drained catchments (Pell et al., 1997; Lancaster et al., 2002; Maroulis et al., 2007; Vermeesch et al., 2010). Many studies have investigated sediment routing dynamics in continental-scale transport systems associated with collisional orogens (Clift et al., 2008; East et al., 2015; Rittner et al., 2016; Garzanti et al., 2017; Wang et al., 2018). However, an understanding of how climatically influenced eolian systems affect sediment routing across orogenic systems remains an outstanding problem in sediment systems research (Muhs and Zárate, 2001; Latrubesse et al., 2012; Tripaldi and Zárate, 2016; Mason et al., 2019).

Forecasting and characterizing sediment supply in continental drainage systems reflects the interplay of multiple interdependent variables as sediment is transported from erosional source to the accumulating sink (**Figure 1**). Detrital zircon (DZ) U-Pb geochronology provenance signatures have been integrated into sediment routing studies to track source-to-sink system response to tectonic, climatic, and anthropogenic forcings (Dickinson and Gehrels, 2008; Mackey et al., 2012; Blum and Pecha, 2014; Fildani et al., 2016; Sharman et al., 2017; Blum et al., 2018; Horton, 2018; Sickmann et al., 2019). While numerous studies have explored signal propagation in modern fluvial environments (e.g., Amidon et al., 2005; Saylor et al., 2013; Horton et al., 2015; Capaldi et al., 2017; Jackson et al., 2019; Mason et al., 2019), few have explored how subsequent eolian transport, the primary transport mechanism in arid regions, either integrates, removes, or propagates tectonic signals. Additionally, the eolian record is likely to be especially fragmentary because both accumulation and preservation are characterized by a complex balance between sediment supply,

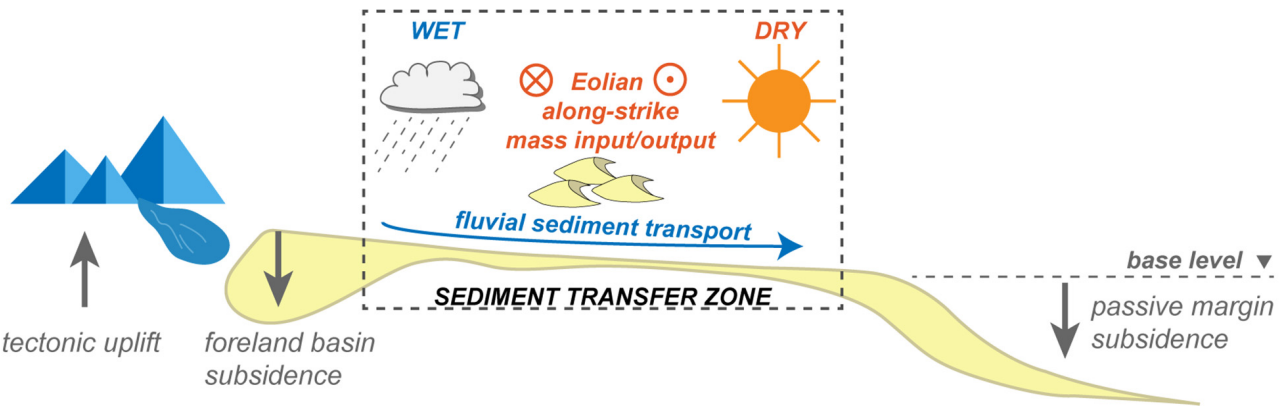

FIGURE 1 | Schematic 2-D profile of the Andean-to-Atlantic margin sediment-routing system of central Argentina emphasizing erosion, transfer, and accumulation zones and important controls of tectonics, climate, base level, and along strike along-strike eolian processes (modified after Romans et al., 2016).

sediment availability and the transport capacity of the wind (Kocurek and Lancaster, 1999; Rodríguez-López et al., 2014). Nevertheless, DZ geochronology is employed on ancient eolian strata to interpret paleoclimatic signals and tectonic events (e.g., Soreghan et al., 2008; Levina et al., 2014; Lawton et al., 2015; Peri et al., 2016; George et al., 2019; Lawton, 2019). This study assesses how modern to Quaternary eolian systems in central Argentina drive either remobilization or storage of Andean river sediment, ultimately feeding or starving down track changes in slope basin systems along the distal Atlantic margin. To quantify the influence of eolian transport in continental drainage systems we: (1) use sediment fingerprinting methods for sand-sized fractions (DZ U-Pb geochronology), (2) incorporate sediment mixing models, and (3) correlate the findings to the regional geomorphology. The Pleistocene to present day Andean Piedmont sand dune fields west central Argentina (Iriondo, 1990; **Figure 2**) offers an ideal location to evaluate the role of eolian influenced transfer zones on sediment routing due in part to well preserved sand dune geomorphology (Tripaldi et al., 2010) and clearly defined Andean tectonic provinces with DZ U-Pb age signatures (Capaldi et al., 2017). Using our results, we assess the relative contributions from fluvial point sources that are reworked and transported within orogen-parallel dune fields, and constrain how tectonic signals are transmitted or modified in eolian conditions induced by climatic shifts. Examining how provenance signatures are propagated through modern source-to-sink systems and preserved in the stratigraphic record will shed light on comparable ancient systems.

GEOLOGIC AND GEOMORPHIC SETTING

Fluvial Megafans of the Argentina Andes

Active sedimentation in the proximal Andean foreland basin of west-central Argentina (31–33°S; **Figure 2A**) is dominated by fluvial megafans fed by large catchments (>10,000 km^2) with localized entry points into the basin, which include the Río Mendoza, Río San Juan, and Río Bermejo fluvial systems (**Figure 2B**). These rivers feed the Río Desaguadero, an axial fluvial system with broad floodplains and ephemeral lagoonal environments that flows southward into the Río Colorado, which ultimately routes Andean orogenic sediment eastward to the distal Atlantic passive margin (**Figure 2A**).

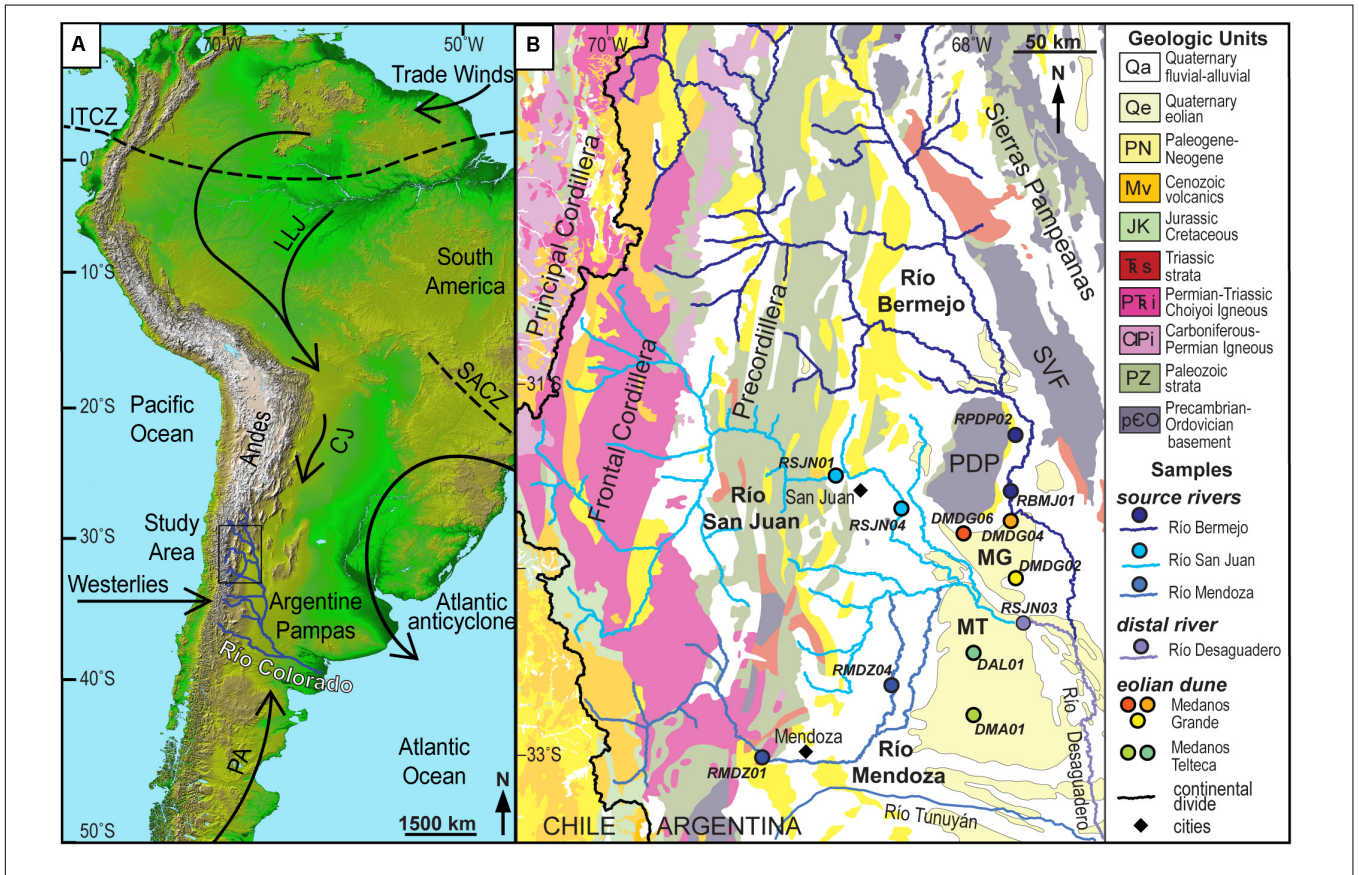

FIGURE 2 | (A) Topographic relief map of South America highlighting Río Colorado sediment routing network and regional wind currents (black lines), Intertropical Convergence Zone (ITCV), Low Level Jet (LLJ), South American Convergent Zone (SACZ), Chaco Jet (CJ), Polar Advections (PA) (modified from Tripaldi and Forman, 2016). **(B)** Geologic map of west-central Argentina indicating the tectonic provinces, fluvial networks (blue lines), and modern river and eolian sample locations (colored circles). Medanos Telteca (MT), Medanos Grande (MG), Sierra Pie de Palo (PDP), Sierra Valle Fértil (SVF).

The Río Mendoza drains high-elevation watersheds dominated by Frontal Cordillera hinterland sources. The Andean hinterland is predominantly composed of reverse-fault blocks that exhume late Paleozoic–Triassic granodiorite intrusions and associated andesitic and rhyolitic lavas, ignimbrites, and pyroclastic rocks of the Choiyoi Igneous complex (unit PTri **Figure 2B**; Heredia et al., 2002). In the west, the Principal Cordillera along the Chile-Argentina border consists of Neogene volcanic and volcaniclastic materials derived from the Andean arc (unit Mv) and deformed Mesozoic rift-related strata (unit JK) (**Figure 2B**; Cristallini and Ramos, 2000; Mackaman-Lofland et al., 2019).

The Río San Juan is fed by an integrative trellis drainage network spanning the Precordillera fold-thrust belt involving a Paleozoic marine clastic and carbonate succession (units PZ) (Ramos, 1988; von Gosen, 1992). Neogene foreland basin deposits (unit PN) are preserved in footwall blocks of major thrust faults with preferential erosion forming intermontane valleys between thrust-generated ranges (Jordan et al., 2001; Levina et al., 2014; Capaldi et al., 2017).

Distal eastern portions of the basin are structurally partitioned by roughly NNW-trending basement-cored uplifts (Sierras Pampeanas) and intervening subsiding zones within a broken foreland basin province. The flanking Río Bermejo flows southward along the western ranges of the Sierras Pampeanas, sourcing broadly folded Triassic-Jurassic fluvial red beds and underlying exhumed Precambrian-lower Paleozoic basement (units Trs and unit PcO) along the Sierra Valle Fertile (SVF; **Figure 2B**) and Sierra Pie de Palo uplifts (PDP; **Figure 2B**), as well as Neogene basin fill (unit PN), and modern alluvial fans along basin-bounding structures (Damanti, 1993).

Holocene Andean Foreland Eolian Dune Fields

The central foreland basin is dominated by a >10,000 km^2 north-trending zone of eolian landforms, including the southern Medanos Telteca and northern Medanos Grande eolian dune fields (**Figure 2B**). Both Medanos Telteca and Grande systems have been estimated to be last active during the Holocene, exhibiting high-relief (50 m) parallel ridges of dominantly longitudinal (seif) dunes and asymmetric transverse dunes, and litharenite to feldspathic litharenite sand composition (Iriondo, 1999; Zárate, 2003; Zárate and Tripaldi, 2012; Tripaldi et al., 2013; Tripaldi and Forman, 2016; Tripaldi and Zárate, 2016). Detailed optically stimulated luminescence (OSL) geochronology has been established across the major eolian provinces of central Argentina, providing a framework to analyze sediment transport across the sediment routing system during the Holocene (Tripaldi and Forman, 2007, 2016; Latrubesse and Ramonell, 2010).

The study region is characterized by low precipitation and winds from the west and southeast. Precipitation in western Argentina is associated with monsoon-type circulation that is generated by humid air masses from the Atlantic anticyclone, and is concentrated (>70%) during October to March. Precipitation decreases from east to west; from 90 to 100 cm/year in the northeastern Pampas to <25–30 cm/year in the Andean piedmont study area (Compagnucci et al., 2002; Tripaldi and Forman, 2016). Regionally, wind conditions are controlled by the subtropical high-pressure cells (Pacific and Atlantic anticyclones), which modulates the Westerlies and Polar advection wind activity. In general, Westerly (Zonda) winds are generated off the Andes and are dominant along the downslope Andean piedmont, and southeasterly Polar Advection (Pampero) winds prevail throughout the year across the eastern Argentine Pampas (**Figure 2A**).

METHODOLOGIES

Detrital Zircon U-Pb Geochronology

We collected and analyzed five Holocene eolian sands sampled at dune crests in the Medanos Telteca (DMA01, DAL01) and Medanos Grande (DMDG02, DMDG06, DMDG04) dune fields, and two modern river sands sampled along active channel bedforms from a tributary of the Río Bermejo (RPDP02) and main trunk of the Río San Juan (RSJN04). U-Pb DZ geochronological data are integrated with previously published U-Pb age results from modern foreland river deposits of Río Mendoza (RMDZ01 and RMDZ04), Río San Juan (RSJN01 and RSJN03), and Río Bermejo (RBMJ01) (Capaldi et al., 2017; **Figure 2**). Standard mineral separation techniques included water table, heavy-liquid density, and magnetic susceptibility separations for all samples. Non-magnetic heavy mineral separates were poured onto double sided tape on 1" epoxy resin mounts and zircon grains were chosen randomly for analysis by laser ablation–inductively coupled plasma–mass spectrometry (LA-ICP-MS) to obtain zircon U-Pb ages. Sample mounts were loaded into a large-volume HelEx sample cell and analyzed with a single-collector, magnetic sector Element 2 ICP-MS with a Photon Machine Analyte G2 excimer laser (Horton et al., 2016; Odlum et al., 2019). Corrections for depth-dependent, elemental and isotopic fractionation were performed using zircon standards GJ1 (600.4 ± 0.1 Ma; Jackson et al., 2004), and secondary standards Plešovice (PL-1; 337.2 ± 0.4 Ma; Sláma et al., 2008; Whitehouse, 2008), and 91500 (1065 Ma; Wiedenbeck et al., 1995). Zircon U-Pb ages and 2σ uncertainty (**Supplementary Table S1**) are reported for analyses with less than 10% $^{206}Pb/^{238}U$ uncertainties, less than 30% discordance, and less than 5% reverse discordance. Reported dates and percent discordance for grains younger than 850 Ma are $^{206}Pb/^{238}U$ ages and discordance $^{206}Pb/^{238}U$ vs. $^{207}Pb/^{235}U$, and for grains older than 850 Ma ages are $^{207}Pb/^{206}Pb$ dates with $^{206}Pb/^{238}U$ vs. $^{207}Pb/^{206}Pb$ discordance.

Results are organized based on spatial relationship among eolian samples from south to north with U-Pb ages for individual samples displayed as probability density functions (PDF), kernel density estimates (KDE) with set bandwidth of 15 Myr, and histogram age bins of 25 Myr. Zircon U-Pb age distributions are described in terms of broad age components of modes for samples that reflect particular Andean provenance signatures. The relative percentage for each of the six age groups are calculated for each fluvial and eolian sample

(**Supplementary Table S2**). Diagnostic age components are as follows, from oldest to youngest.

(1) Proterozoic 1450–950 Ma basement ages have a minor component of 1450–1350 Ma ages recycled from the Laurentian-derived Cuyania terrane. Dominate 1200–950 Ma Sunsás (Grenville) age component are sourced from numerous metamorphic basement units across the western Sierras Pampeanas and are ubiquitous in most Ordovician to Permian sedimentary sequences from the Precordillera (Ramos, 2004, 2009; Bahlburg et al., 2009; Rapela et al., 2016);
(2) The Eastern Sierras Pampeanas (725–520 Ma) age group are recycled from Carboniferous to Permian sedimentary sequences found in the Precordillera fold-thrust belt (Fosdick et al., 2015; Capaldi et al., 2017). The Eastern Sierras Pampeanas (725–520 Ma) age group is composed of a minor 725–540 Ma age component initially recycled from sourced from metasedimentary rocks (Puncoviscana Formation) and a dominant 538–515 Ma age peak from Cambrian rocks of the Pampean magmatic arc (Rapela et al., 2007; Schwartz et al., 2008);
(3) The Western Sierras Pampeanas (510–380 Ma) age group is derived from sources throughout the western Sierras Pampeanas involving 495–440 Ma Famatinian continental arc rocks and subsequent 460–385 Ma metamorphic assemblages (Mulcahy et al., 2014; Otamendi et al., 2017). Recycled Western Sierras Pampeanas 510–380 Ma DZ age components are derived from Carboniferous-Permian sedimentary units in the Precordillera fold-thrust belt and Triassic sedimentary sequences overlying western Sierras Pampeanas uplifts (Capaldi et al., 2017);
(4) Late Paleozoic 375–280 Ma zircon ages are from minor 360–335 Ma igneous suite spanning the study area and dominate 340–280 Ma Carboniferous arc rocks of the Principal and Frontal Cordilleras (Mpodozis and Kay, 1992; Dahlquist et al., 2013) and minor recycled sources from Triassic sedimentary deposits in the Sierras Pampeanas and Neogene deposits throughout the Frontal Cordillera, and Precordillera (Fosdick et al., 2015, 2017);
(5) Permian Triassic 280–205 Ma age group includes dominant Choiyoi Igneous Complex and subsequent Triassic plutons exposed in the Frontal Cordillera (**Figure 2B**; Mpodozis and Kay, 1992; del Rey et al., 2016). Additional sources of Permian Triassic 280–205 Ma age components include recycled Jurassic to Cretaceous sedimentary deposits in the High Andes and Neogene deposits across the Precordillera (Capaldi et al., 2017; Mackaman-Lofland et al., 2019);
(6) Andean Arc 120–0 Ma Cretaceous to Neogene Andean arc volcanic and volcaniclastic rocks of the Principal Cordillera, Frontal Cordillera, Precordillera, and Sierras Pampeanas, and recycled from Neogene basin fill (Kay and Mpodozis, 2002; Jones et al., 2015).

Comparison among fluvial and eolian sand samples DZ U-Pb age distributions was accomplished by visual inspection of the relative abundance of age groups (**Supplementary Table S2**), and using commonly applied metrics of similarity using PDFs, KDEs, and cumulative distribution functions (CDFs) (**Supplementary Table S3**). Comparison among DZ PDF and KDE employed cross-plot (R^2 cross-correlation coefficient), Similarity, and Likeness. Whereas statistical test on CDF age distributions included Kolmogorov-Smirnov (K-S) test (D value), and Kuiper's test (V value). We apply these comparative methods using the program DZ Stats (Saylor and Sundell, 2016). The relative measure of similarity among age distributions provide quantitative comparison metrics to determine whether samples were drawn from the same parent population and degree of similarity between sample age distributions. For this study we utilize R^2 cross-correlation coefficient on KDEs, which is sensitive to the number and relative proportions of detrital age modes and more discriminating than other test (Saylor and Sundell, 2016). Additional DZ U-Pb age distributions comparison was established through metric multidimensional scaling (MDS) plots to identify greater similarity for samples that cluster together and less similar for those that plot farther apart. Metric MDS is applied by constructing a pairwise dissimilarity matrix of detrital age distributions among the fluvial and eolian samples using R^2 cross-correlation coefficient. Metric MDS plot and results was created using the program DZmds (Saylor et al., 2018).

Sediment DZ "unmixing" modeling approaches allow for discrimination of the potential proportions of different contribution sources mixed in eolian and fluvial transport using the DZmix program (Sundell and Saylor, 2017). Mixture modeling of DZ U-Pb data was used to determine the contributions of sediment sources from the three fluvial systems (i.e., Río Mendoza, Río San Juan, and Río Bermejo) by randomly mixing potential fluvial source age distribution KDEs and comparing model output to target downstream eolian and river sand samples DZ age distribution. The mixing model determines a range of best mixtures of potential sources using an inverse Monte Carlo approach of randomly scaling each source age distribution by a random set of percent contributions that sum to 100%, summing the scaled distributions to give a single model distribution and quantitatively comparing that model distribution to a eolian or river sample distribution through R^2 cross correlation. This process is repeated 100,000 times for each basin sample KDE, and the best 1000 model fits (1%) are used to calculate the mean and standard deviation (1σ) contribution from each potential source (**Supplementary Table S4**).

RESULTS

Detrital Zircon Age Distributions

Fluvial Megafan Sediment Input

Detrital zircon U-Pb age distributions from modern river sands in the southern Central Andean foreland demonstrate distinctive age signatures from several competing sediment inputs, including the Río Mendoza and Río San Juan fluvial megafans, which have been shown to accurately reflect the distribution of source units within retroarc hinterland and

thrust belt catchment areas. DZ ages from the broken foreland drainage network along the Río Bermejo axial trunk river represent local contributions from foreland basement-cored uplifts of the Sierras Pampeanas (**Figure 2B**; Capaldi et al., 2017). This well-characterized modern river age distributions provides a valuable opportunity to apply DZ provenance results to track sediment mixing and redistribution by fluvial and eolian processes within a sediment transfer zone between source and sink.

The southern Río Mendoza fluvial megafan consists of modern river drainage networks that source Neogene Andean volcanic rocks and the Choiyoi Permian-Triassic volcanic complex. The composite DZ U-Pb age spectra (samples RMDZ04 and RMDZ01) is dominated by a bimodal Permian-Triassic (280–205 Ma) and late Paleozoic (375–280 Ma) age populations with all other diagnostic ages being nearly absent (**Figure 3**). The strong bimodal DZ age signature from the Río Mendoza is indicative of hinterland volcanic material derived from the Frontal Cordillera, which is inferred to be representative of the age signature for the more southern Río Tunuyán (**Figure 2B**).

The western Río San Juan fluvial megafan is fed by the Precordillera fold-thrust belt, which reflects erosion and recycling of Paleozoic and Neogene basin fill, and upstream hinterland volcanic sources in the Frontal Cordillera. Detrital zircon U-Pb results from Río San Juan (samples RSJN01 and RSJN04) show multimodal age distribution that include Andean arc (<120 Ma) and Permian-Triassic arc (280–205 Ma) age components indicating recycling from exhumed Neogene strata between Precordillera thrust sheets. Additionally, significant Eastern Sierras Pampeanas (725–520 Ma) and Proterozoic (1450–925 Ma) age zircon grains are derived from the recycling of Paleozoic sedimentary sequences from the core of the thrust sheets (**Figure 3**).

The northern Río Bermejo megafan drains the western Sierras Pampeanas basement-involved uplifts in the distal reach of an expansive drainage network encompassing Precordillera and Frontal Cordillera source. The DZ age distributions from modern river sands (samples RPDP02 and RBMJ01) that includes western Sierras Pampeanas (510–380 Ma), Eastern Sierras Pampeanas (725–520 Ma), and Proterozoic (1450–925 Ma) age groups. Age distributions dominated by older> 350

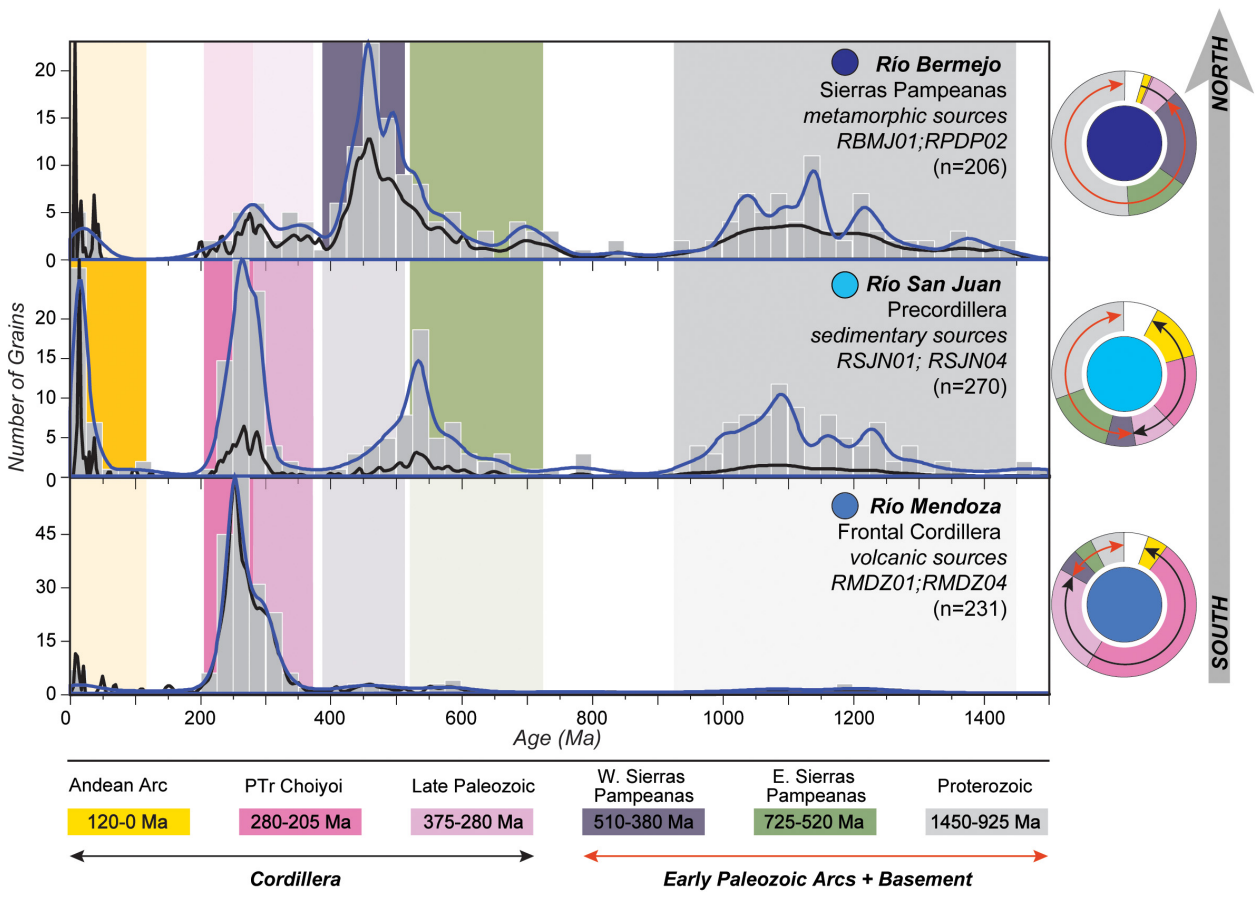

FIGURE 3 | Comparative plot of detrital zircon (DZ) U-Pb age distributions for modern river sands, depicted as age histograms (gray rectangles), kernel density estimates (blue line), and relative probability density plots (black line), with emphasis on key age populations (dark color shading) and minor to no age populations (transparent color shading). Donut diagrams represent percent abundance of key age populations in each sample, with Cordillera (black arrows) and Early Paleozoic Arcs and Basement (red arrow) age groups emphasized, and inner colored circle corresponds to sample locations in **Figure 2B**.

Ma age populations are indicative of sediment recycling of both the overlaying Mesozoic strata and exhumed Ordovician-Precambrian crystalline basement cores of the active western Sierras Pampeanas uplifts rather than hinterland age signatures (**Figures 2B**, **3**; Capaldi et al., 2017).

Fluvial-Eolian Transfer Zone Deposits

The fluvial sediment sources southern Río Mendoza, western Río San Juan, and northern Río Bermejo deliver sediment to the Andean foreland proximal to the Holocene eolian system (**Figures 2**, **5B**). New DZ age distributions from eolian sand samples are compared to proximal fluvial sand samples to distinguish spatial variations in Andean signals in relationship to contradictory south-flowing rivers and north-directed wind patterns (**Figure 4**). Results demonstrate the ability to track sedimentary signals from Andean rivers across the Holocene eolian Andean foreland, and compare observed Holocene spatial patterns to modern fluvial signatures (RSJN03).

The southern Medanos Telteca eolian field is proximal to the Río Mendoza and Río Tunuyán fluvial megafan system draining the Frontal Cordillera volcanic units. Both southern and northern Medanos Telteca samples DMA01 and DAL01 exhibit similar DZ U-Pb age distributions that are characterized by dominant (26–27%) Permian-Triassic (280–205 Ma) age peak, subordinate (18–21%) Proterozoic ages, and minor (8–17%) late Paleozoic (375–280 Ma) Western and Eastern Sierras Pampeanas (510–380 Ma and 725–520 Ma) populations (**Figure 4**). Comparison with fluvial megafan inputs yield cross correlation R^2 coefficient results that indicate higher similarity (0.71–0.75 R^2 values) with Río Mendoza age distributions, and moderate similarity (0.54–0.57 R^2 values) with Río San Juan (**Table 1**).

The northern Medanos Grande eolian field is located between the Río San Juan and Río Bermejo fluvial systems, these rivers erode predominantly Neogene age sedimentary sequences and Paleozoic metasedimentary units in the Precordillera and crystalline basement rocks along the Sierras Pampeanas (**Figure 2B**). In general, Medanos Grande eolian deposits (DMDG02, DMDG04, and DMDG06) exhibit greater abundances of older zircon ages (>380 Ma) than samples from the southern Medanos Telteca (**Figure 4**). The DZ age distributions from Medanos Grande samples are dominated by (25–31%) Proterozoic ages and (20–29%) Western Sierras Pampeanas (510–380 Ma) age populations, with subordinate amounts (8–17%) of late Paleozoic (375–280 Ma) and Eastern Sierras Pampeanas (725–520 Ma), and minor components (7–10%) of Andean arc (<120 Ma) and Permian-Triassic (280–205 Ma) age populations (**Figure 4**). Medanos Grande samples are compared with each fluvial megafan sample age distributions, which yield moderately-low similarity (0.21–0.34 R^2 values) with Río Bermejo composite age signature (**Table 1**). However, the southern Medanos Grande sample DMDG02 exhibits moderate similarity (>0.35 R^2 values) with Río Mendoza fluvial source, than samples DMDG04 and DMDG06 from northern and western Medanos Grande that show low similarity with Río Mendoza (<0.2 R^2 values). Medanos Grande samples (DMDG02, DMDG04, DMDG06) are moderately similar (0.29 to 0.50 R^2 values) to Río San Juan age distribution.

Modern river sample RSJN03 reflects the geomorphic transition from Río Mendoza and Río San Juan fluvial megafan, to distal Río Desaguadero axial river headwaters (**Figure 2B**). The DZ age distribution contains strong (24%) late Paleozoic (375–280 Ma) and (23%) Proterozoic age populations, with subordinate (12–16%) Permian-Triassic (280–205 Ma), Western and Eastern Sierras Pampeanas (510–380 Ma and 725–520 Ma), and minor (8%) Andean arc ages (**Figure 4**). The distal fluvial sample DZ spectrum is similar to Río Mendoza (0.61 R^2 value) and Río San Juan (0.57 R^2 value), and dissimilar to Río Bermejo age distribution (0.02 R^2 value) (**Table 1**).

Fluvial-Eolian DZ Sample Comparison

Comparisons among the three diagnostic fluvial megafan DZ age distributions and Holocene eolian DZ age distributions show complementary south-to-north mixing trends (**Table 1** and **Supplementary Table S3**). Specifically, R^2 cross-correlation coefficient values from eolian sample comparison with fluvial source display a south-to-north decrease in similarity with Mendoza fluvial megafan samples, where southern Medanos Telteca samples DMA01 and DAL01 has high R^2 values of 0.71–0.75 and northern Medanos Grande samples DMDG have low R^2 values of 0.1–0.35 (**Table 1**). Comparison of eolian samples with Bermejo fluvial megafan samples yield an inverse trend of south to north increase in R^2 cross-correlation coefficient values, from low R^2 values 0.02–0.04 for southern Medanos Telteca samples to relatively higher R^2 values 0.2 to 0.34 in northern Medanos Grande. However, sample comparison among eolian and Río San Juan fluvial samples only exhibit a slight south to north decrease R^2 values from 0.57 to 0.3 (**Table 1**).

A clear trend appears from the CDF plot, where the eolian samples DZ age distributions uniquely plot between the Río Mendoza, Río San Juan, and Río Bermejo fluvial megafan sediment input samples (**Figure 5A**). Comparing trends among eolian samples reveals a progressive variation from southern Medanos Telteca samples (DMZ01 and DAL01) and northern Medanos Grande (DMDG). Cenozoic to Mesozoic age segments of the eolian CDFs plot between Río San Juan and Río Mendoza for the southern Medanos Telteca samples and the northern Medanos Grande samples plot between Río San Juan and Río Mendoza CDFs (**Figure 5A**). Paleozoic age segments of all the eolian CDFs plot between Río Bermejo and Río Mendoza where southern Medanos Telteca samples are most similar to Río Mendoza and the northern Medanos Grande samples plot closer to Río Bermejo CDF. Precambrian age segments of the southern Medanos Telteca samples are most similar to Río Mendoza and the northern Medanos Grande samples plot closer to Río San Juan CDF (**Figure 5A**). These CDF age distribution trends indicate fluvial inputs are end members in terms of DZ age distributions, which further suggests the eolian deposits contain mixed age distributions from the fluvial sources.

Detrital zircon samples from the Andean foreland transfer zone were compared to each other and to the fluvial megafan composite age distributions using two-dimensional (2D) MDS plot (**Figure 5B**). The misfit from conversion of sample dissimilarity to disparity in Cartesian space via linear transformation gives a good correlation as indicated by a low

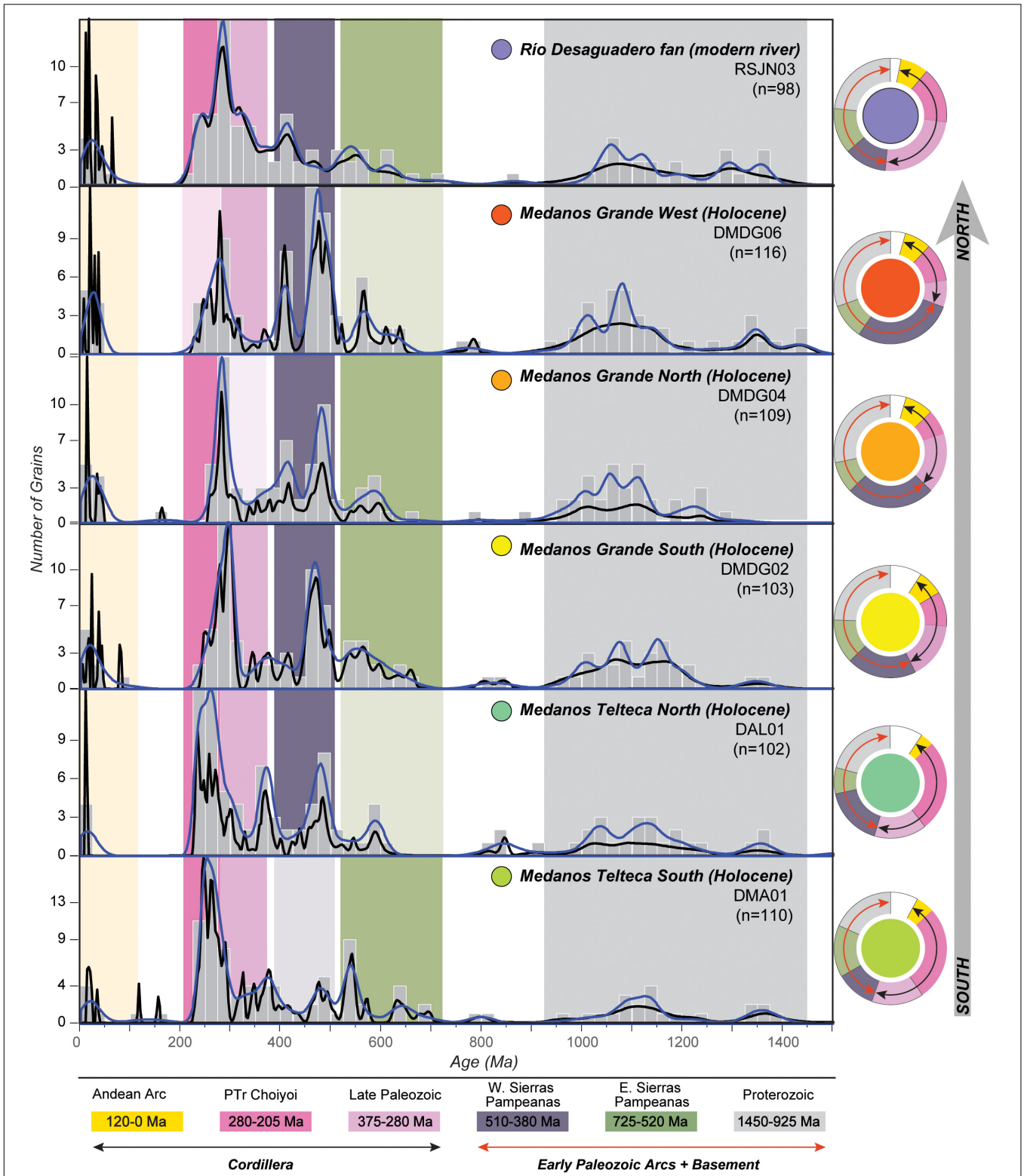

FIGURE 4 | Comparative plot of DZ U-Pb age distributions for Holocene eolian samples and modern river sand, depicted as age histograms (gray rectangles), kernel density estimates (blue line) and relative probability density plots (black line), with emphasis on key age populations (dark color shading) and minor to no age populations (transparent color shading). Donut diagrams represent percent abundance of key age populations in each sample, with Cordillera (black arrows) and Early Paleozoic Arcs and Basement (red arrow) age groups emphasized, and inner colored circle corresponds to sample locations in **Figure 2B**.

TABLE 1 | Inter sample KDE cross correlation R^2 coefficient results.

	Mendoza	San Juan	Bermejo	DMA01	DAL01	RSJN03	DMDG02	DMDG04	DMDG06
Mendoza	1	0.52	0.01	0.71	0.75	0.61	0.35	0.1	0.19
San Juan	0.52	1	0.09	0.54	0.57	0.57	0.5	0.3	0.43
Bermejo	0.01	0.09	1	0.02	0.04	0.02	0.21	0.34	0.34
DMA01	0.71	0.54	0.02	1	0.81	0.57	0.45	0.23	0.35
DAL01	0.75	0.57	0.04	0.81	1	0.64	0.62	0.39	0.5
RSJN03	0.61	0.57	0.02	0.57	0.64	1	0.57	0.38	0.35
DMDG02	0.35	0.5	0.21	0.45	0.62	0.57	1	0.75	0.69
DMDG04	0.1	0.3	0.34	0.23	0.39	0.38	0.75	1	0.77
DMDG06	0.19	0.43	0.34	0.35	0.5	0.35	0.69	0.77	1

Darker red shading indicates greater R^2 value.

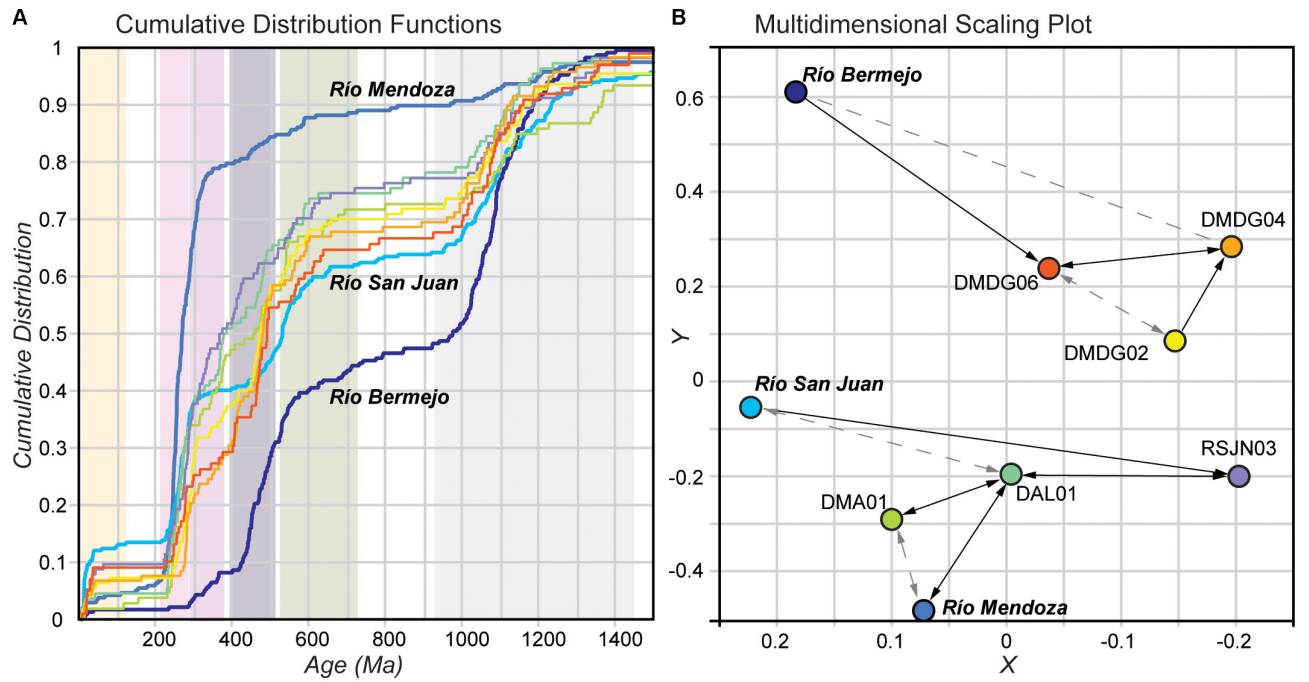

FIGURE 5 | Comparison plots of fluvial sources (blue and labeled) and eolian mixed samples (color coded and labeled). **(A)** Detrital zircon U-Pb age distribution cumulative density functions (CDF), where line color corresponds to colored circles in **B** and sample locations in **Figure 2B**, with emphasis on key age populations (color shading). Notice all samples plot in between fluvial sources Río Mendoza and Río Bermejo in CDF space. **(B)** Two-dimensional multidimensional scaling (MDS) plot of detrital zircon U-Pb age distributions generated for river sources and mixed eolian samples using R2 cross-correlation coefficient on KDEs. Lines represent nearest neighbor (black lines), second nearest neighbor (gray dashed line), and axis are unitless.

stress minimal (0.09). Results show that Medanos Telteca samples are most similar to each other and to Río Mendoza source (**Figure 5B**). Medanos Grande samples DMDG02, DMDG04, and DMDG06 are the most similar to Río Bermejo. The distal foreland fluvial fan sample RSJN03 uniquely plots in MDS space away from Holocene eolian samples, with closet neighbor being upstream composite samples of Río San Juan and closest eolian sample DAL01.

DZ Mixing Model Results

The mixing model results for the Holocene eolian and modern river sand using KDE Cross Correlation R^2 similarity metric show a similar progressive mixing of south to north fluvial sources (**Figure 6** and **Supplementary Table S4**). Modeled age distributions indicate that the southern parent source Río Mendoza decreased from 56 to 14% south to north. In contrast, northern Río Bermejo sediment input is shown to increased northward from 18 to 64%. An apparent outlier to this trend is sample DAL04 that shows a stark decrease in Río San Juan contribution to 4%, relative to nearest eolian samples that show 31% in DMA01 and 30% in DMDG02 Río San Juan contribution. Whereas modeled age distribution for the modern distal foreland sample (RSJN03) shows comparable contribution among Río Mendoza (44%), Río San Juan (31%), Río Bermejo (25%) (**Figure 6**). The CDF based mixing model results (i.e., Kuiper's test V value and K-S test D value) also show similar

trends to that of KDE and PDP based models, with higher Río Mendoza proportion in southern Medanos Grande samples (∼50%), in contrast Río Bermejo signature dominated the northern Medanos Telteca samples (56 to 63%) (**Supplementary Table S4**). However, the Río San Juan component in the CDF based mixing model results are low and invariant, where the Río San Juan component in the Kuiper's test ranges from 2 to 10% and the K-S test ranges from 8 to 13%, compared to the 20–37% range from the KDE based mixing models. Due to the observed CDF based mixing model insensitivity with multimodal Río San Juan source age distribution, the discussion focuses on the KDE Cross-Correlation mixing model results and trends. In summary, the results from each modeling approach indicate a Holocene south-north progressive mixing of fluvial sources, and modern mixed fluvial sample displays more proportional contribution from each fluvial megafan source.

DISCUSSION

Holocene Eolian Sediment Mixing Along Orogen Parallel Paleocurrents

Fluvial point sources at the orogenic front carry primary tectonic signals, reflecting the bedrock material of their respective Andean catchments (**Figure 3**; Capaldi et al., 2017). These fluvial megafans deliver sediment downstream to the Argentina foreland sediment transfer zone that is controlled by fluvial-alluvial and eolian processes during the Holocene. As tectonic signals enter the transfer zone, eolian processes become more dominant and modify the primary fluvial signals, thereby diluting tectonic signals across climate-driven paleoflow directions (**Figure 7**).

Each eolian sample DZ age distribution contains contributions from all fluvial point sources indicating substantial mixing and homogenization by eolian transport and reworking. These results are also supported by the sediment mixing model which suggests that signals from the Río Mendoza, Bermejo, and San Juan are represented in all eolian samples (**Figure 4**). Despite the persistence of similar age modes between eolian samples (e.g., **Figure 5A**), defined spatial and temporal mixing trends persist. Generally, eolian samples taken from the southernmost portion of the dune fields in the Medanos Telteca, proximal to the Río Mendoza, reflect the highest proportions of sediment derived from the Río Mendoza, while samples taken from the northern portions of the Medanos Grande dune field reflect the highest proportions of sediment from the proximal Río Bermejo (**Figure 6**).

Holocene dune crest orientations are useful for understanding the south-north trend in the DZ age distributions. Both the Medanos Telteca and Medanos Grande dune fields display prominent longitudinal (sheif) sand dune morphologies (**Figure 7**). Longitudinal dunes parallel the resultant vector of two paleocurrents that typically have 40° between the two converging vectors (Tsoar, 1983; Bristow et al., 2000). Longitudinal dunes form in wide unimodal or bi-directional wind regimes so the resultant vector transport direction is approximately parallel to the dune trend, and tend to flow parallel with river direction (Liu and Coulthard, 2015). The southern Medanos Telteca longitudinal dunes trend ∼320° in the south-southwestern region and ∼280° in the distal western edge. The northern Medanos Grande longitudinal dunes trend ∼290° in the southern tip and progressively trends to ∼315° in the northwest region and ∼355° in the northern tip (**Figure 7**). From the longitudinal dune trends two paleocurrent directions can be interpreted to involve winds that flowed from the Andes to the east (i.e., Westerlies/Zonda) and winds that flowed along Pampas plain to the north-northwest (i.e., Polar Advection/Pampero; **Figure 2A**). Modern wind data collected show a strong south to southwesterly component with a resultant drift potential of winds capable of transporting sands is due north at 352° (**Figure 7B**; Tripaldi and Forman, 2007).

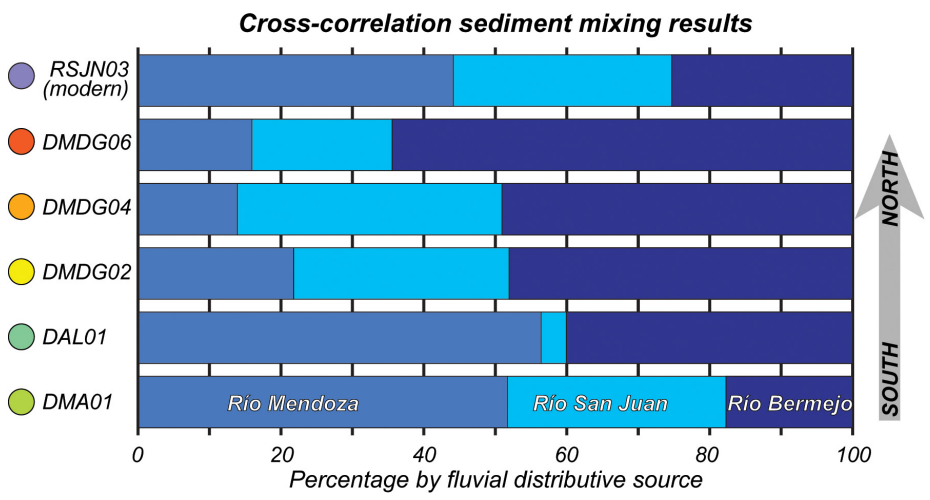

FIGURE 6 | DZ age distribution mixing model results for Holocene eolian and modern distal fluvial samples comparing the relative contribution (in%) from Río Bermejo, Río San Juan, and Río Mendoza age distributions using KDE R^2 cross-correlation coefficient test. Note south to north trend in Holocene eolian samples and equal proportioned modern distal fluvial sample (RSJN03).

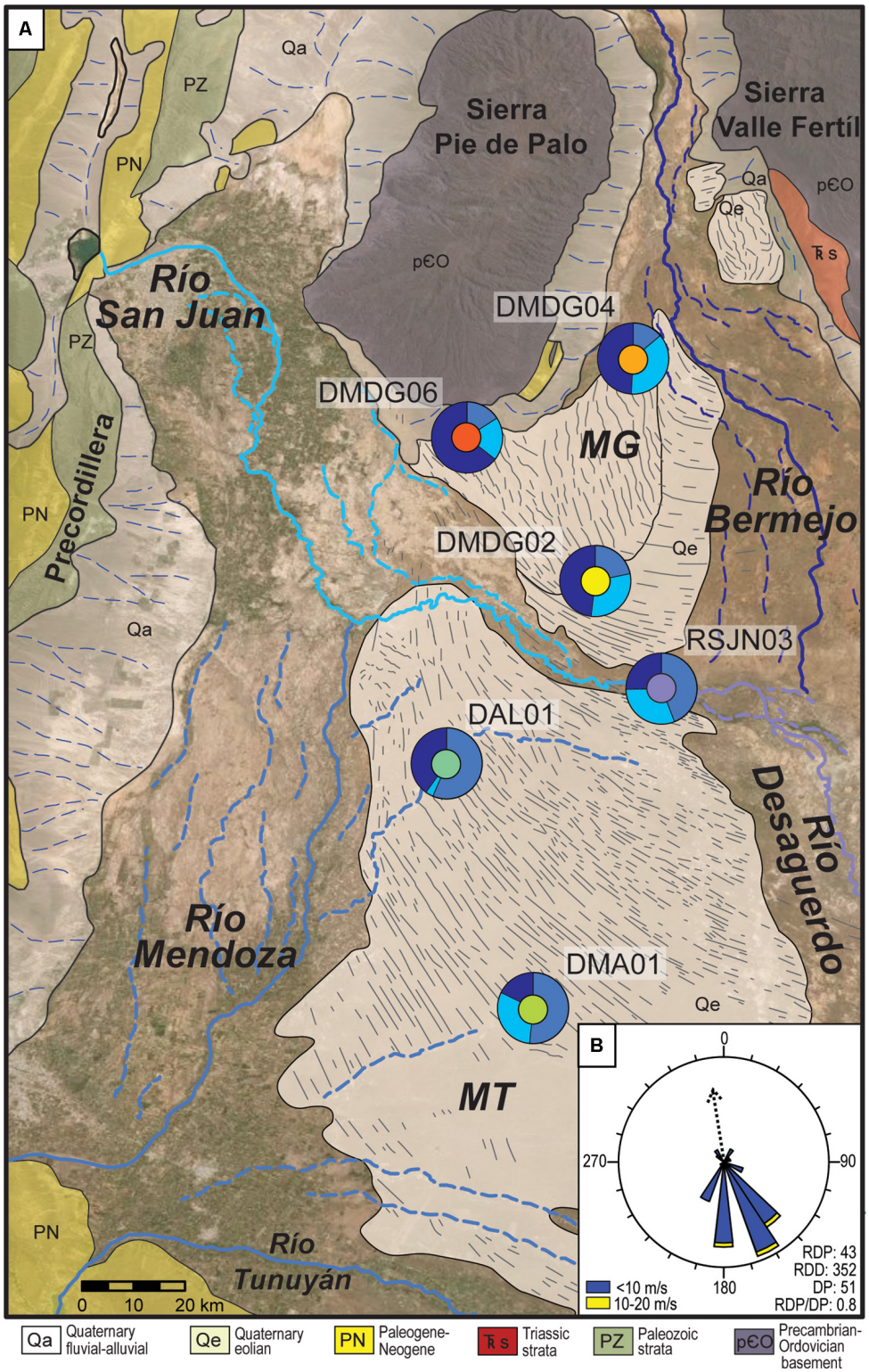

FIGURE 7 | Geomorphic map of eolian and fluvial megafan systems in Andean foreland sediment transfer zone. **(A)** Holocene eolian and modern distal fluvial samples detrital zircon mixing model results are plotted as donut diagrams (see **Figure 6**), where Medanos Telteca (MT) and Medanos Grande (MG) sands have distinct mixed proportions of fluvial megafan sediment inputs. **(B)** Rose diagram of modern wind vectors collected from San Juan that are capable of transporting sand-sized sediments (<10 and 10–20 m/s) (modified from Tripaldi and Forman, 2007).

Integrating Holocene paleocurrent vectors with DZ age distribution mixing models provide a mechanism for the mixing of fluvial megafan signatures observed in the eolian deposits (**Figure 7**). The Andean southerly winds explain the reworking and transport of southern Río Mendoza fluvial megafan deposits northward across the Medanos Telteca and into the northern Medanos Grande. Similarly, the Polar Advection/Pampero southeasterly winds helps account for the presence of Río Bermejo and Río San Juan fluvial age signatures in the southern Medanos Telteca dune field that increase in the northern Medanos Grande dune field. The presence of northern Río Bermejo and northwestern Río San Juan signatures in the southern Medanos Telteca eolian samples is likely from reworked deposits along the axial-fluvial Río Desaguadero eastern floodplain (**Figure 7A**). Overall these results show that sediment fluxes in the Argentine foreland are controlled by a combination of fluvial and eolian processes, whose relative importance can be assessed with DZ U-Pb geochronology. Importantly, eolian transport has the potential to overprint primary tectonic signals, but in this case, leaves a resolvable mixing trend along the Holocene paleo-wind vector.

Aridification Drives Orogen Parallel Eolian Activity

The driver of eolian activity can be linked to Quaternary climate variability and increased aridity in the Andean foreland and Argentine Pampas plain during the Holocene (Iriondo, 1999). Quaternary glacial/interglacial cycles drove regional wind systems to change strength and latitudinal positions, affecting their capacity for erosion and transport of sand and mineral dust from the sources to depositional areas (**Figure 8**; Gili et al., 2017). Eolian deposition spans most of the Holocene to ca. 400 years ago, associated with an inferred mean annual precipitation of 100–450 mm and drier conditions compared to the late 20th century (Tripaldi and Forman, 2016). Holocene eolian events along the Andean foreland are well constrained with OSL geochronology and have occurred over 4.3–4, 2.1, and 0.6–0.4 ka (**Figure 8A**; Tripaldi and Forman, 2007). Eolian activity is synchronous with local Andean glacial advances during 4.3–4.7, 2.5–2.2, and 0.4–0.3 ka intervals (**Figure 8B**; Espizua, 2005; Espizua and Pitte, 2009). The shared temporal histories of both Holocene Andean glaciation and eolian deposition suggest that the Argentina sediment transfer zone is sensitive to changes in regional climate regimes.

Changes to global circulation cells driven by sea surface temperature change is a potential mechanism for the variable wet and arid Quaternary climates recorded by the transfer zone deposits. In the Andean foreland dune fields, winds capable of transporting sand-sized sediments are controlled by the South Atlantic Anticyclone and the low-level meridional Chaco Jet (**Figure 2A**; Forman et al., 2014). Wet conditions in western Argentina are associated with cooler sea surface temperatures in the equatorial South Atlantic Ocean and strengthened South Atlantic Convergent Zone and Chaco Low Level jets, increasing the landward flux of Atlantic-derived moisture (Doyle and Barros, 2002). Dry conditions appear to be associated with higher sea surface temperatures that lead to a weakened South Atlantic Convergent Zone and more zonal transport of moisture by the Chaco Low Level Jet toward southeastern Brazil (Liebmann et al., 2004). Migration of the Chaco jet eastward reduces South American monsoonal moisture entering the Andean Piedmont of Argentina, increasing aridification, and decreasing fluvial transport capacity.

Understanding eolian system processes from historical ($<10^3$ year) to intermediate Pleistocene-Holocene (10^3–10^6) year time periods provides invaluable characterization that can be applied to ancient ($>10^7$ year) systems in the stratigraphic record (Allen, 2008). For example, Miocene aridity (from ca. 6.1 to 5.2 Ma) is recorded by numerous stable isotope proxies from stratigraphic and fossil records (Ruskin and Jordan, 2007; Hynek et al., 2012; Pingel et al., 2016). Miocene aridity is

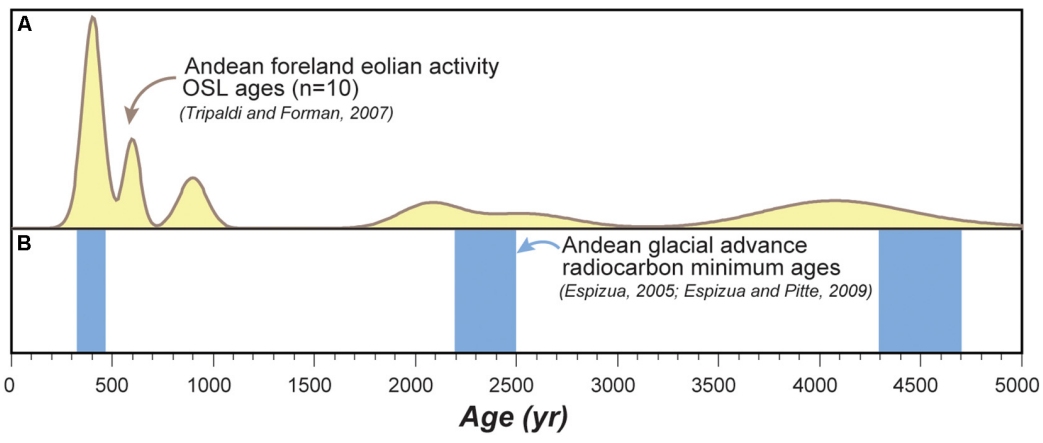

FIGURE 8 | Holocene chronology of eolian and glacial activity in NW Argentina. **(A)** Optically Stimulated luminescence (OSL) ages from Andean Piedmont eolian fields Medanos Grande and Medanos Negros located east of Sierra Valle Fertile (**Figure 7** for location; Tripaldi and Forman, 2007). **(B)** Radiocarbon minimum ages from terminal moraine glacial deposits in the Andes of Mendoza province (Espizua, 2005; Espizua and Pitte, 2009). Note the overlap between glacial advance and subsequent eolian activity.

expressed as a decrease in fluvial sedimentation and erosion rates, without preservation of eolian strata (Amidon et al., 2017; Stevens Goddard and Carrapa, 2018). Preserved Oligocene-Miocene eolian strata along the southern Central Andes (Tripaldi and Limarino, 2005; Levina et al., 2014; Fosdick et al., 2017) suggest a protracted history of fluctuating arid conditions in this region throughout the Cenozoic. Moreover, a thorough understanding of processes operating in eolian systems is important for predicting how these regions will continue to evolve as anthropogenic warming and increased agricultural development continues to shape the Earth's landscape, resource management, and human land use (Munson et al., 2011; Sickmann et al., 2019).

Tectonic and Climate Signal Propagation in Fluvial-Eolian Transfer Zones

The Andean foreland basin and associated fluvial-eolian sediment transfer zone serves as an intermediate terrestrial sink that modulates sedimentary delivery to the Atlantic passive margin. During wet periods with high precipitation rates, the regionally integrated fluvial drainage systems serve as the primary mechanism for transporting sediment through the transfer zone to offshore sinks. Sediment mixing in these fluvial systems generally reflects equal contributions from fluvial point sources flowing southward (**Figure 9A**). During times of high precipitation, fluvial sediment should accurately reflect the bedrock lithologies being eroded, thereby preserving the tectonic signals in the transfer zone fluvial sediments (DeCelles and Hertel, 1989; Capaldi et al., 2017). Climatic shifts toward more arid conditions may activate eolian transport and cause integrated drainages to dry up, leaving only fluvial megafans and ephemeral streams (**Figure 9B**). During intensely arid climatic conditions, eolian transport would be the primary transport mechanism in transfer zones and would mix sediment along prevailing wind vectors, producing a climatic signal in the sedimentary record (**Figure 9B**). Northward orogen-parallel sediment mixing initiated by eolian transport during arid climate periods likely disrupted an otherwise simple pattern of southward fluvial transport within the foreland basin. By inhibiting fluvial sediment transfer downstream to the Río Desaguadero axial system and Río Colorado en route to the Atlantic margin, eolian redistribution and mixing of sediment likely modified the original Andean orogenic signals recognized in rivers of the proximal foreland basin.

Sediment signal propagation depends on the timescales of tectonic and climatic perturbations influencing sediment discharge and the capacity of a system to response to those changes (Romans et al., 2016). Numerical models predict that the erosional dynamics of mountain catchments significantly dampen the transfer of sediment discharge variations driven by high frequency (~105 year) climate oscillations (Armitage et al., 2013). This suggests that sediment routing systems operate over the long term (millions of years) as consistent conveyors of sediment to distal zones of accumulation and are less sensitive climate signals (Castelltort and Van Den Driessche, 2003; Allen, 2008). Others have shown that large low-gradient foreland settings increase sediment signal buffering

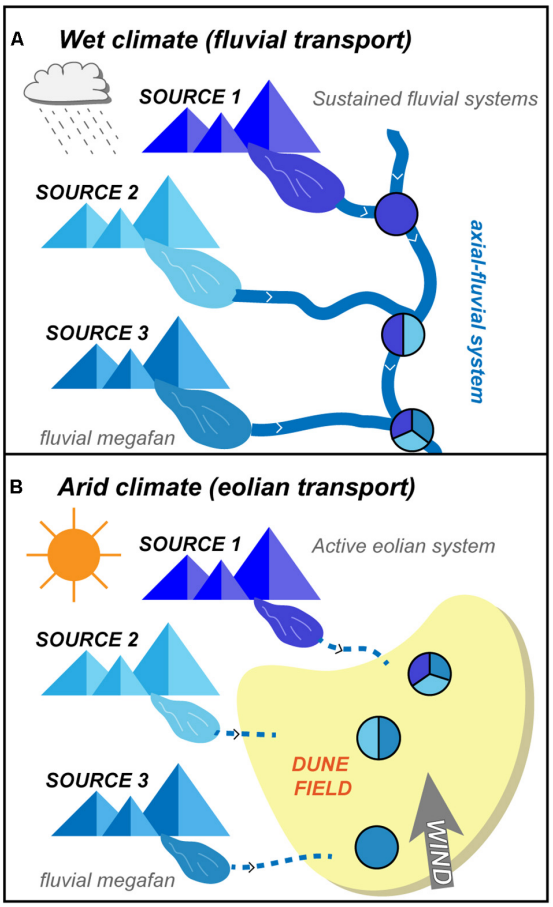

FIGURE 9 | Schematic depiction of three distinct environmental signals propagated from their source regions and transported by fluvial sediment-routing networks to distal eolian systems in an arid foreland basin. Hypothetical fluvial signatures are indicated by pie diagrams according to the respective sample location. **(A)** Fluvial-dominated end-member sediments contain signals dominated by the provenance of the river sources that mix southward along confluences. **(B)** Simplified eolian-dominated end-member where fluvial megafan deposits are reworked northward along orogen parallel wind currents.

(Jerolmack and Paola, 2010) and decrease the potential to transfer a source sediment signal to the ultimate sink (Covault et al., 2013; Nyberg et al., 2018). However, climate shifts may drive significant longer-term changes in transport mechanisms within long-lived continental systems that are sensitive to climate variations on intermediate timescales (<106 year) (Goodbred, 2003; Simpson and Castelltort, 2012). Our results show that climatically modulated eolian activity in the foreland basin prevents a simple downslope propagation of tectonic signals through the Andean transfer zone. Similar findings from other fluvial and eolian transport systems indicate that sediment storage in the eolian system can inhibit or delay environmental signal propagation from the orogenic sources to the ultimate sink (East et al., 2015). Future work collecting provenance and geochronology constraints along downstream Río Desaguadero and Río Colorado fluvial and eolian systems would provide

additional insights into how environmental signatures propagate throughout the Quaternary sediment transfer zone.

Understanding environmental signal propagation through fluvial-eolian sedimentary transfer zones over 10^2 to 10^5 years timescales sheds light on how strengthened wind transport and/or weakening of the hydrological cycle impacted sediment routing and potentially inhibited transmission of unambiguous tectonic signals from source to sink. During drier conditions, the sediment transport direction is reversed and sediment is redistributed northward by orogen-parallel paleowinds, which rework and disrupt the original tectonic signals exiting the erosional domain of the Andean orogen (**Figure 9B**). Importantly, these results suggest that eolian environments generally induce sediment mixing over 10^2 to 10^4 years timescales, and preserve regional, rather than local, records of erosion in adjacent source regions. Wetter interglacial periods display provenance signatures indicative of fluvial transport from southward, preserving Andean tectonic signatures (**Figure 9A**). Our data show promise of recording climatic conditions in foreland settings and provide a basis for understanding how fluvial-eolian transport processes interact and impact signal propagation through a continental-scale drainage network linking a major orogenic belt to a distal passive margin.

CONCLUSION

We investigated a Holocene sediment transfer zone with contrasting fluvial and eolian sediment transport mechanisms to understand how river and wind processes impact the propagation of environmental signals in continental-scale drainage systems. Detrital zircon U-Pb age distributions from Holocene eolian dunes record the progressive sediment mixing of the three fluvial point sources along a norward trend. In contrast, modern river sands show progressive southward (downstream) mixing along a large axial fluvial system. Reversal in sediment transport directions indicates that sediment routing networks in the Andean transfer zone are sensitive to changes in regional climate regimes. South flowing fluvial systems are characteristic of wet inter-glacial periods, whereas northward eolian transport, preserved by dune crest morphology, is prevalent during Holocene glaciation in the central Andes. Sediment mixing induced by eolian transport and reworking of various synorogenic river sediment is likely a critical, climate-modulated process that inhibits downstream transmission of primary Andean tectonic signals to distal zones of accumulation.

DATA AVAILABILITY STATEMENT

All datasets generated for this study are included in the article/**Supplementary Material**.

AUTHOR CONTRIBUTIONS

TC designed the project and carried out the field work. JH, TC, and SG processed the samples, and carried out the analysis and data interpretation. DS facilitated the geochronology analysis. TC, SG, and JH wrote the manuscript. BH and DS provided critical discussions and contributions to the manuscript.

FUNDING

This research was funded by the Geological Society of America, American Association of Petroleum Geologists, Society for Sedimentary Geology, and Jackson School of Geosciences at The University of Texas at Austin (Grants awarded to TC).

ACKNOWLEDGMENTS

We thank Margo Odlum, Mark Helper, Sharon Mosher, Patricia Alvarado, and Gustavo Ortiz for discussions and logistical assistance in Argentina. This manuscript benefited from discussions with Brian Romans, Edgardo Latrubesse, David Mohrig, Ryan Anderson, and Lisa Stockli. We are grateful for the constructive reviews and comments from reviewers PV and KS, and the editor JF, which improved the manuscript.

SUPPLEMENTARY MATERIAL

The Supplementary Material for this article can be found online at: https://www.frontiersin.org/articles/10.3389/feart.2019.00298/full#supplementary-material

TABLE S1 | Detrital zircon U-Pb results.

TABLE S2 | Percentage age group.

TABLE S3 | Statistical coefficient results.

TABLE S4 | Mixing model results.

REFERENCES

Allen, P. A. (2008). Time scales of tectonic landscapes and their sediment routing systems. *Geol. Soc. Lon. Spe. Publ.* 296, 7–28. doi: 10.1144/sp296.2

Al-Masrahy, M. A., and Mountney, N. P. (2015). A classification scheme for fluvial–aeolian system interaction in desert-margin settings. *Aeolian Res.* 17, 67–88. doi: 10.1016/j.aeolia.2015.01.010

Amidon, W. H., Burbank, D. W., and Gehrels, G. E. (2005). U-Pb zircon ages as a sediment mixing tracer in the Nepal Himalaya. *Earth Planet. Sci. Lett.* 235, 244–260. doi: 10.1016/j.epsl.2005.03.019

Amidon, W. H., Fisher, G. B., Burbank, D. W., Ciccioli, P. L., Alonso, R. N., Gorin, A. L., et al. (2017). Mio-pliocene aridity in the south-central Andes associated with Southern Hemisphere cold periods. *Proc. Natl. Acad. Sci. U.S.A.* 114, 6474–6479. doi: 10.1073/pnas.1700327114

Armitage, J. J., Jones, T. D., Duller, R. A., Whittaker, A. C., and Allen, P. A. (2013). Temporal buffering of climate-driven sediment flux cycles by transient catchment response. *Earth Planet. Sci. Lett.* 369, 200–210. doi: 10.1016/j.epsl.2013.03.020

Bahlburg, H., Vervoort, J. D., Du Frane, S. A., Bock, B., Augustsson, C., and Reimann, C. (2009). Timing of crust formation and recycling in accretionary

orogens: insights learned from the western margin of South America. *Earth Sci. Rev.* 97, 215–241. doi: 10.1016/j.earscirev.2009.10.006

Belnap, J., Munson, S. M., and Field, J. P. (2011). Aeolian and fluvial processes in dryland regions: the need for integrated studies. *Ecoydrology* 4, 615–622. doi: 10.1002/eco.258

Blum, M., and Pecha, M. (2014). Mid-cretaceous to paleocene North American drainage reorganization from detrital zircons. *Geology* 42, 607–610. doi: 10.1130/g35513.1

Blum, M., Rogers, K., Gleason, J., Najman, Y., Cruz, J., and Fox, L. (2018). Allogenic and autogenic signals in the stratigraphic record of the deep-sea bengal fan. *Sci. Rep.* 8:7973. doi: 10.1038/s41598-018-25819-5

Bristow, C. S., Bailey, S. D., and Lancaster, N. (2000). The sedimentary structure of linear sand dunes. *Nature* 406, 56–59. doi: 10.1038/35017536

Bullard, J. E., and McTainsh, G. H. (2003). Aeolian-fluvial interactions in dryland environments: examples, concepts and Australia case study. *Progress Phys. Geogr.* 27, 471–501. doi: 10.1191/0309133303pp386ra

Capaldi, T. N., Horton, B. K., McKenzie, N. R., Stockli, D. F., and Odlum, M. L. (2017). Sediment provenance in contractional orogens: the detrital zircon record from modern rivers in the Andean fold-thrust belt and foreland basin of western Argentina. *Earth Planet. Sci. Lett.* 479, 83–97. doi: 10.1016/j.epsl.2017.09.001

Castelltort, S., and Van Den Driessche, J. (2003). How plausible are high-frequency sediment supply-driven cycles in the stratigraphic record? *Sediment. Geol.* 157, 3–13. doi: 10.1016/s0037-0738(03)00066-6

Clift, P. D., Hodges, K. V., Heslop, D., Hannigan, R., Van Long, H., and Calves, G. (2008). Correlation of Himalayan exhumation rates and Asian monsoon intensity. *Nat. Geosci.* 1, 875–880. doi: 10.1038/ngeo351

Compagnucci, R. H., Agosta, E. A., and Vargas, W. M. (2002). Climatic change and quasi-oscillations in central-west Argentina summer precipitation: main features and coherent behaviour with southern African region. *Clim. Dyn.* 18, 421–435. doi: 10.1007/s003820100183

Covault, J. A., Craddock, W. H., Romans, B. W., Fildani, A., and Gosai, M. (2013). Spatial and temporal variations in landscape evolution: historic and longer-term sediment flux through global catchments. *J. Geol.* 121, 35–56. doi: 10.1086/668680

Cristallini, E. O., and Ramos, V. A. (2000). Thick-skinned and thin-skinned thrusting in the La Ramada fold and thrust belt: crustal evolution of the High Andes of San Juan, Argentina (32°SL). *Tectonophysics* 317, 205–235. doi: 10.1016/s0040-1951(99)00276-0

Dahlquist, J. A., Pankhurst, R. J., Gaschnig, R. M., Rapela, C. W., Casquet, C., Alasino, P. H., et al. (2013). Hf and Nd isotopes in Early Ordovician to Early Carboniferous granites as monitors of crustal growth in the proto-Andean margin of Gondwana. *Gondwana Res.* 23, 1617–1630. doi: 10.1016/j.gr.2012.08.013

Damanti, J. F. (1993). Geomorphic and structural controls on facies patterns and sediment composition in a modern foreland basin. *Spec. Publ. Int. Ass. Sediment.* 17, 221–233.

DeCelles, P. G., and Hertel, F. (1989). Petrology of fluvial sands from the Amazonian foreland basin. Peru and Bolivia. *GSA Bull.* 101, 1552–1562. doi: 10.1130/0016-7606(1989)101<1552:pofsft>2.3.co;2

del Rey, A., Deckart, K., Arriagada, C., and Martínez, F. (2016). Resolving the paradigm of the late Paleozoic–Triassic Chilean magmatism: isotopic approach. *Gondwana Res.* 37, 172–181. doi: 10.1016/j.gr.2016.06.008

Dickinson, W. R., and Gehrels, G. E. (2008). Sediment delivery to the Cordilleran foreland basin: insights from U-Pb ages of detrital zircons in upper jurassic and cretaceous strata of the Colorado Plateau. *Am. J. Sci.* 308, 1041–1082.

Doyle, M. E., and Barros, V. R. (2002). Midsummer low-level circulation and precipitation in subtropical South America and related sea surface temperature anomalies in the South Atlantic. *J. Clim.* 15, 3394–3410. doi: 10.1175/1520-0442(2002)015<3394:MLLCAP>2.0.CO;2

East, A. E., Clift, P. D., Carter, A., Alizai, A., and VanLaningham, S. (2015). Fluvial-eolian interactions in sediment routing and sedimentary signal buffering: an example from the Indus basin and Thar desert. *J. Sediment. Res.* 85, 715–728. doi: 10.2110/jsr.2015.42

Espizua, L. E. (2005). Holocene glacier chronology of valenzuela valley, Mendoza Andes, Argentina. *Holocene* 15, 1079–1085. doi: 10.1191/0959683605hl866rr

Espizua, L. E., and Pitte, P. (2009). The little ice age glacier advance in the central Andes (35°S), Argentina. *Palaeogeogr. Palaeoclimatol. Palaeoecol.* 281, 345–350. doi: 10.1016/j.palaeo.2008.10.032

Fildani, A., Hessler, A. M., Mason, C. C., McKay, M. P., and Stockli, D. F. (2018). Late pleistocene glacial transitions in North America altered major river drainages, as revealed by deep-sea sediment. *Sci. Rep.* 8:13839. doi: 10.1038/s41598-018-32268-7

Fildani, A., McKay, M. P., Stockli, D., Clark, J., Dykstra, M. L., Stockli, L., et al. (2016). The ancestral mississippi drainage archived in the late wisconsin mississippi deep-sea fan. *Geology* 44, 479–482. doi: 10.1130/g37657.1

Forman, S. L., Tripaldi, A., and Ciccioli, P. L. (2014). Eolian sand sheet deposition in the San Luis paleodune field, western Argentina as an indicator of a semi-arid environment through the Holocene. *Palaeogeogr. Palaeoclimatol. Palaeoecol.* 411, 122–135. doi: 10.1016/j.palaeo.2014.05.038

Fosdick, J. C., Carrapa, B., and Ortíz, G. (2015). Faulting and erosion in the Argentine Precordillera during changes in subduction regime: reconciling bedrock cooling and detrital records. *Earth Planet. Sci. Lett.* 431, 73–83. doi: 10.1016/j.epsl.2015.09.041

Fosdick, J. C., Reat, E. J., Carrapa, B., Ortiz, G., and Alvarado, P. M. (2017). Retroarc basin reorganization and aridification during Paleogene uplift of the southern central Andes. *Tectonics* 36, 493–514. doi: 10.1002/2016TC004400

Garzanti, E., Resentini, A., Andò, S., Vezzoli, G., Pererira, A., and Vermeesch, P. (2015). Physical controls on sand composition and relative durability of detrital minerals during ultra-long distance littoral and aeolian transport (Namibia and southern Angola). *Sedimentology* 62, 971–996. doi: 10.1111/sed.12169

Garzanti, E., Vermeesch, P., Al-Ramadan, K. A., AndÒ, S., Limonta, M., Rittner, M., et al. (2017). Tracing transcontinental sand transport: from Anatolia–zagros To the Rub'Al Khali Sand Sea. *J. Sediment. Res.* 87, 1196–1213. doi: 10.2110/jsr.2017.65

George, S. W., Horton, B. K., Jackson, L. J., Moreno, F., Carlotto, V., and Garzione, C. N. (2019). "Sediment provenance variations during contrasting mesozoic-early cenozoic tectonic regimes of the northern Peruvian Andes and Santiago-Marañón foreland basin," in *Andean Tectonics*, eds B. K. Horton, and A. Folguera, (Cambridge, MA: Elsevier), 269–296. doi: 10.1016/b978-0-12-816009-1.00012-5

Gili, S., Gaiero, D. M., Goldstein, S. L., Chemale, F. Jr., Jweda, J., Kaplan, M. R., et al. (2017). Glacial/interglacial changes of Southern Hemisphere wind circulation from the geochemistry of South American dust. *Earth Planet. Sci. Lett.* 469, 98–109. doi: 10.1016/j.epsl.2017.04.007

Goodbred, S. L. Jr. (2003). Response of the ganges dispersal system to climate change: a source-to-sink view since the last interstade. *Sediment. Geol.* 162, 83–104. doi: 10.1016/s0037-0738(03)00217-3

Heredia, N., Rodriguez-Fernandez, L. R., Gallastegui, G., Busquets, P., and Colombo, F. (2002). Geological setting of the argentine frontal cordillera in the flat-slab segment (30°00'–31°30'S latitude. *J. South Am. Earth Sci.* 15, 79–99. doi: 10.1016/s0895-9811(02)00007-x

Horton, B. K. (2018). Sedimentary record of Andean mountain building. *Earth Sci. Rev.* 178, 279–309. doi: 10.1016/j.earscirev.2017.11.025

Horton, B. K., Anderson, V. J., Caballero, V., Saylor, J. E., Parra, M., and Mora, A. (2015). Application of detrital zircon U-Pb geochronology to surface and subsurface correlations of provenance, paleodrainage, and tectonics of the middle magdalena valley Basin of Colombia. *Geosphere* 11, 1790–1811. doi: 10.1130/ges01251.1

Horton, B. K., Fuentes, F., Boll, A., Starck, D., Ramirez, S. G., and Stockli, D. F. (2016). Andean stratigraphic record of the transition from backarc extension to orogenic shortening: a case study from the northern Neuquén Basin, Argentina. *J. South Am. Earth Sci.* 71, 17–40. doi: 10.1016/j.jsames.2016.06.003

Hynek, S. A., Passey, B. H., Prado, J. L., Brown, F. H., Cerling, T. E., and Quade, J. (2012). Small mammal carbon isotope ecology across the Miocene–Pliocene boundary, northwestern Argentina. *Earth Planet. Sci. Lett.* 321, 177–188. doi: 10.1016/j.epsl.2011.12.038

Ingersoll, R. V., Kretchmer, A. G., and Valles, P. K. (1993). The effect of sampling scale on actualistic sandstone petrofacies. *Sedimentology* 40, 937–953. doi: 10.1111/j.1365-3091.1993.tb01370.x

Iriondo, M. (1990). The map of the South American plains. Its present state. *Quat. South Am. Anct. Pen* 6, 297–306.

Iriondo, M. (1999). Climatic changes in the South American plains: records of a continent-scale oscillation. *Quat. Int.* 57, 93–112. doi: 10.1016/s1040-6182(98)00053-6

Jackson, L. J., Horton, B. K., and Vallejo, C. (2019). Detrital zircon U-Pb geochronology of modern Andean rivers in Ecuador: fingerprinting tectonic provinces and assessing downstream propagation of provenance signals. *Geosphere* 15. doi: 10.1130/GES02126.1

Jackson, S. E., Pearson, N. J., Griffin, W. L., and Belousova, E. A. (2004). The application of laser ablation-inductively coupled plasma-mass spectrometry to in situ U-Pb zircon geochronology. *Chem. Geol.* 211, 47–69. doi: 10.1016/j.chemgeo.2004.06.017

Jerolmack, D. J., and Paola, C. (2010). Shredding of environmental signals by sediment transport. *Geophys. Res. Lett.* 37, 1–5.

Johnsson, M. J., Stallard, R. F., and Lundberg, N. (1991). Controls on the composition of fluvial sands from a tropical weathering environment: sands of the Orinoco river drainage basin, Venezuela and Colombia. *GSA Bull.* 103, 1622–1647. doi: 10.1130/0016-7606(1991)103<1622:cotcof>2.3.co;2

Johnsson, M. J., Stallard, R. F., and Meade, R. H. (1988). First-cycle quartz arenites in the Orinoco River basin. Venezuela and Colombia. *J. Geol.* 96, 263–277. doi: 10.1086/629219

Jones, R. E., Kirstein, L. A., Kasemann, S. A., Dhuime, B., Elliott, T., Litvak, V. D., et al. (2015). Geodynamic controls on the contamination of Cenozoic arc magmas in the southern Central Andes: insights from the O and Hf isotopic composition of zircon. *Geochim. Cosmoch. Acta* 164, 386–402. doi: 10.1016/j.gca.2015.05.007

Jordan, T. E., Schlunegger, F., and Cardozo, N. (2001). Unsteady and spatially variable evolution of the Neogene Andean Bermejo foreland basin. Argentina. *J. South Am. Earth Sci.* 14, 775–798. doi: 10.1016/s0895-9811(01)00072-4

Kay, S. M., and Mpodozis, C. (2002). Magmatism as a probe to the Neogene shallowing of the Nazca plate beneath the modern Chilean flat-slab. *J. South Am. Earth Sci.* 15, 39–57. doi: 10.1016/s0895-9811(02)00005-6

Kocurek, G., and Ewing, R. C. (2012). "Source-to-sink: an earth/mars comparison of boundary conditions for eolian dune systems," in *Sedimentary Geology of Mars*, eds J. P. Grotzinger, and R. E. Milliken, (Tulsa, OK: Society for Sedimentary Geology), 151–168. doi: 10.2110/pec.12.102.0151

Kocurek, G. A., and Lancaster, N. (1999). Aeolian system sediment state: theory and mojave desert dune field example. *Sedimentology* 46, 505–515. doi: 10.1046/j.1365-3091.1999.00227.x

Lancaster, N., Kocurek, G., Singhvi, A., Pandey, V., Deynoux, M., Ghienne, J. F., et al. (2002). Late pleistocene and holocene dune activity and wind regimes in the western Sahara Desert of Mauritania. *Geology* 30, 991–994.

Latrubesse, E. M., and Ramonell, C. G. (2010). Landforms and chronology in the Pampean Sand Sea, Argentina. *Int. Sediment. Congress* 18:529.

Latrubesse, E. M., Stevaux, J. C., Cremon, E. H., May, J. H., Tatumi, S. H., Hurtado, M. A., et al. (2012). Late quaternary megafans, fans and fluvio-aeolian interactions in the Bolivian Chaco, Tropical South America. *Palaeogeogr. Palaeoclimatol., Palaeoecol.* 356, 75–88. doi: 10.1016/j.palaeo.2012.04.003

Lawton, T. F. (2019). "Transient influences upon late Paleozoic sediment provenance and dispersal in Laurentian Pangea," in *GSA Annual Meeting in Phoenix*, (Arizona).

Lawton, T. F., and Buck, B. J. (2006). Implications of diapir-derived detritus and gypsic paleosols in lower triassic strata near the castle valley salt wall. Paradox Basin, Utah. *Geology* 34, 885–888.

Lawton, T. F., Buller, C. D., and Parr, T. R. (2015). Provenance of a permian erg on the western margin of Pangea: depositional system of the Kungurian (late Leonardian) castle valley and white rim sandstones and subjacent cutler group, paradox basin, Utah, USA. *Geosphere* 11, 1475–1506. doi: 10.1130/ges01174.1

Levina, M., Horton, B. K., Fuentes, F., and Stockli, D. F. (2014). Cenozoic sedimentation and exhumation of the foreland basin system preserved in the Percordillera thrust belt (31-32°S), south central Andes, Argentina. *Tectonics* 33, 1659–1680. doi: 10.1002/2013TC003424

Liebmann, B., Vera, C. S., Carvalho, L. M. V., Camilloni, I. A., Hoerling, M. P., Allured, D., et al. (2004). An observed trend in central South American precipitation. *J. Clim.* 17, 4357–4367. doi: 10.1175/3205.1

Liu, B., and Coulthard, T. J. (2015). Mapping the interactions between rivers and sand dunes: implications for fluvial and aeolian geomorphology. *Geomorphology* 231, 246–257. doi: 10.1016/j.geomorph.2014.12.011

Mackaman-Lofland, C., Horton, B. K., Fuentes, F., Constenius, K. N., and Stockli, D. F. (2019). Mesozoic to cenozoic retroarc basin evolution during changes in tectonic regime, southern Central Andes (31–33°S): Insights from zircon U-Pb geochronology. *J. South Am. Earth Sci.* 89, 299–318. doi: 10.1016/j.jsames.2018.10.004

Mackey, G. N., Horton, B. K., and Milliken, K. L. (2012). Provenance of the paleocene-eocene wilcox group, western gulf of mexico basin: evidence for integrated drainage of the southern laramide rocky mountains and cordilleran arc. *GSA Bull.* 124, 1007–1024. doi: 10.1130/b30458.1

Maroulis, J. C., Nanson, G. C., Price, D. M., and Pietsch, T. (2007). Aeolian-fluvial interaction and climate change: source-bordering dune development over the past 100 ka on cooper creek, central Australia. *Quat. Sci. Rev.* 26, 386–404. doi: 10.1016/j.quascirev.2006.08.010

Mason, C. C., Fildani, A., Gerber, T., Blum, M. D., Clark, J. D., and Dykstra, M. (2017). Climatic and anthropogenic influences on sediment mixing in the Mississippi source-to-sink system using detrital zircons: late Pleistocene to recent. *Earth Planet. Scie. Lett.* 466, 70–79. doi: 10.1016/j.epsl.2017.03.001

Mason, C. C., Romans, B. W., Stockli, D. F., Mapes, R., and Fildani, A. (2019). Detrital zircons reveal sea-level and hydroclimate controls on Amazon River to deep-sea fan sediment transfer. *Geology* 47, 563–567. doi: 10.1130/g45852.1

Mehl, A., Tripaldi, A., and Zárate, M. (2018). Late quaternary aeolian and fluvial-aeolian deposits from southwestern Pampas of Argentina, southern South America. *Palaeogeogr. Palaeoclimatol. Palaeoecol.* 511, 280–297. doi: 10.1016/j.palaeo.2018.08.014

Mpodozis, C., and Kay, S. M. (1992). Late paleozoic to triassic evolution of the gondwana margin: evidence from chilean frontal cordilleran batholiths (28 S to 31 S). *Geol. Soc. Am. Bull.* 104, 999–1014. doi: 10.1130/0016-7606(1992)104<0999:lptteo>2.3.co;2

Muhs, D. R., and Zárate, M. (2001). "Late quaternary eolian records of the Americas and their paleoclimatic significance," in *Interhemispheric Climate Linkages*, ed. V. Markgraf, (Amsterdam: Elsevier), 183–216. doi: 10.1016/b978-012472670-3/50015-x

Mulcahy, S. R., Roeske, S. M., McClelland, W. C., Ellis, J. R., Jourdan, F., Renne, P. R., et al. (2014). Multiple migmatite events and cooling from granulite facies metamorphism within the Famatina arc margin of northwest Argentina. *Tectonics* 33, 1–25. doi: 10.1002/2013tc003398

Munson, S. M., Belnap, J., Okin, G. S., and Schlesinger, W. H. (2011). Responses of wind erosion to climate-induced vegetation changes on the Colorado Plateau. *Proc. Natl. Acad. Sci. U.S.A.* 108, 3854–3859. doi: 10.1073/pnas.1014947108

Nyberg, B., Gawthorpe, R. L., and Helland-Hansen, W. (2018). The distribution of rivers to terrestrial sinks: implications for sediment routing systems. *Geomorphology* 316, 1–23. doi: 10.1016/j.geomorph.2018.05.007

Odlum, M. L., Stockli, D. F., Capaldi, T. N., Thomson, K. D., Clark, J., Puigdefàbregas, C., et al. (2019). Tectonic and sediment provenance evolution of the South Eastern Pyrenean foreland basins during rift margin inversion and orogenic uplift. *Tectonophysics* 765, 226–248. doi: 10.1016/j.tecto.2019.05.008

Otamendi, J. E., Ducea, M. N., Cristofolini, E. A., Tibaldi, A. M., Camilletti, G. C., and Bergantz, G. W. (2017). U-Pb ages and Hf isotope compositions of zircons in plutonic rocks from the central Famatinian arc. Argentina. *J. South Am. Earth Sci.* 76, 412–426. doi: 10.1016/j.jsames.2017.04.005

Pell, S. D., Williams, I. S., and Chivas, A. R. (1997). The use of protolith zircon-age fingerprints in determining the protosource areas for some Australian dune sands. *Sediment. Geol.* 109, 233–260. doi: 10.1016/s0037-0738(96)00061-9

Peri, V. G., Naipauer, M., Pimentel, M., and Barcelona, H. (2016). Eolian deposits of the southwestern margin of the Botucatú paleoerg: reconstruction of the gondwana landscape in central northern Argentina. *Sediment. Geol.* 339, 234–257. doi: 10.1016/j.sedgeo.2016.03.019

Pingel, H., Mulch, A., Alonso, R. N., Cottle, J., Hynek, S. A., Poletti, J., et al. (2016). Surface uplift and convective rainfall along the southern Central Andes (Angastaco Basin, NW Argentina). *Earth Planet. Sci. Lett.* 440, 33–42. doi: 10.1016/j.epsl.2016.02.009

Ramos, V. A. (1988). Tectonics of the Late Proterozoic—Early Paleozoic: a collisional history of southern South America. *Episodes* 11, 168–174. doi: 10.18814/epiiugs/1988/v11i3/003

Ramos, V. A. (2004). Cuyania, an exotic block to Gondwana: review of a historical success and the present problems. *Gondwana Res.* 7, 1009–1026. doi: 10.1016/s1342-937x(05)71081-9

Ramos, V. A. (2009). "Anatomy and global context of the Andes: main geologic features and the Andean orogenic cycle," in *Backbone of the Americas: Shallow Subduction, Plateau Uplift, and Ridge and Terrane Collision*, eds S. M. Kay, V. A. Ramos, and W. R. Dickinson, (Boulder, CO: GSA Memoir), 31–65.

Rapela, C. W., Pankhurst, R. J., Casquet, C., Fanning, C. M., Baldo, E. G., González-Casado, J. M., et al. (2007). The Río de la Plata craton and the assembly of SW Gondwana. *Earth Sci. Rev.* 83, 49–82. doi: 10.1016/j.earscirev.2007.03.004

Rapela, C. W., Verdecchia, S. O., Casquet, C., Pankhurst, R. J., Baldo, E. G., Galindo, C., et al. (2016). Identifying laurentian and SW gondwana sources in the Neoproterozoic to early paleozoic metasedimentary rocks of the sierras pampeanas: paleogeographic and tectonic implications. *Gondwana Res.* 32, 193–201.

Rittner, M., Vermeesch, P., Carter, A., Bird, A., Stevens, T., Garzanti, E., et al. (2016). The provenance of Taklamakan desert sand. *Earth Planet. Sci. Lett.* 437, 127–137. doi: 10.1016/j.epsl.2015.12.036

Rodríguez-López, J. P., Clemmensen, L. B., Lancaster, N., Mountney, N. P., and Veiga, G. D. (2014). Archean to recent aeolian sand systems and their sedimentary record: current understanding and future prospects. *Sedimentology* 61, 1487–1534. doi: 10.1111/sed.12123

Romans, B. W., Castelltort, S., Covault, J. A., Fildani, A., and Walsh, J. P. (2016). Environmental signal propagation in sedimentary systems across timescales. *Earth Sci. Rev.* 153, 7–29. doi: 10.1016/j.earscirev.2015.07.012

Ruskin, B. G., and Jordan, T. E. (2007). Climate change across continental sequence boundaries: paleopedology and lithofacies of iglesia basin, Northwestern Argentina. *J. Sediment. Res.* 77, 661–679. doi: 10.2110/jsr.2007.069

Saylor, J. E., Jordan, J. C., Sundell, K. E., Wang, X., Wang, S., and Deng, T. (2018). Topographic growth of the Jishi Shan and its impact on basin and hydrology evolution, NE Tibetan Plateau. *Basin Res.* 30, 544–563. doi: 10.1111/bre.12264

Saylor, J. E., Knowles, J. N., Horton, B. K., Nie, J., and Mora, A. (2013). Mixing of source populations recorded in detrital zircon U-Pb age spectra of modern river sands. *J. Geol.* 121, 17–33. doi: 10.1086/668683

Saylor, J. E., and Sundell, K. E. (2016). Quantifying comparison of large detrital geochronology data sets. *Geosphere* 12, 203–220. doi: 10.1130/ges01237.1

Schwartz, J. J., Gromet, L. P., and Miro, R. (2008). Timing and duration of the calc-alkaline arc of the pampean orogeny: implications for the late neoproterozoic to Cambrian evolution of Western Gondwana. *J. Geol.* 116, 39–61. doi: 10.1086/524122

Sharman, G. R., Covault, J. A., Stockli, D. F., Wroblewski, A. F. J., and Bush, M. A. (2017). Early Cenozoic drainage reorganization of the United States Western Interior–Gulf of Mexico sediment routing system. *Geology* 45, 187–190. doi: 10.1130/g38765.1

Sharman, G. R., Sylvester, Z., and Covault, J. A. (2019). Conversion of tectonic and climatic forcings into records of sediment supply and provenance. *Sci. Rep.* 9, 1–7. doi: 10.1038/s41598-019-39754-6

Sickmann, Z. T., Chheda, T. D., Capaldi, T. N., Thomson, K. D., Paull, C. K., and Graham, S. A. (2019). Using provenance analysis in an Anthropocene natural laboratory. *Quat. Sci. Rev.* 221:105890. doi: 10.1016/j.quascirev.2019.105890

Sickmann, Z. T., Paul, C. K., and Graham, S. A. (2016). Detrital-zircon mixing and partitioning in fluvial to deep marine systems, central California, USA. *J. Sediment. Res.* 86, 1298–1307. doi: 10.2110/jsr.2016.78

Simpson, G., and Castelltort, S. (2012). Model shows that rivers transmit high-frequency climate cycles to the sedimentary record. *Geology* 40, 1131–1134. doi: 10.1130/g33451.1

Sláma, J., Košler, J., Condon, D. J., Crowley, J. L., Gerdes, A., Hanchar, J. M., et al. (2008). Plešovice zircon—a new natural reference material for U–Pb and Hf isotopic microanalysis. *Chem. Geol.* 249, 1–35. doi: 10.1016/j.chemgeo.2007.11.005

Soreghan, M. J., Soreghan, G. S., and Hamilton, M. A. (2008). Glacial-interglacial shifts in atmospheric circulation of western tropical Pangaea. *Palaeogeogr. Palaeoclimatol. Palaeoecol.* 268, 260–272. doi: 10.1016/j.palaeo.2008.03.051

Stevens Goddard, A., and Carrapa, B. (2018). Effects of miocene–pliocene global climate changes on continental sedimentation: a case study from the southern Central Andes. *Geology* 46, 647–650. doi: 10.1130/g40280.1

Sundell, K. E., and Saylor, J. E. (2017). Unmixing detrital geochronology age distributions. *Geochem., Geophys., Geosyst.* 18, 2872–2886. doi: 10.1002/2016GC006774

Tripaldi, A., Ciccioli, P. L., Alonso, M. S., and Forman, S. L. (2010). Petrography and geochemistry of late quaternary dune fields of western Argentina: provenance of aeolian materials in southern South America. *Aeol. Res* 2, 33–48. doi: 10.1016/j.aeolia.2010.01.001

Tripaldi, A., and Forman, S. L. (2007). Geomorphology and chronology of Late Quaternary dune fields of western Argentina. Palaeogeography, Palaeoclimatology. *Palaeoecology* 251, 300–320. doi: 10.1016/j.palaeo.2007.04.007

Tripaldi, A., and Forman, S. L. (2016). Eolian depositional phases during the past 50 ka and inferred climate variability for the Pampean Sand Sea, western Pampas. Argentina. *Quat. Sci. Rev.* 139, 77–93. doi: 10.1016/j.quascirev.2016.03.007

Tripaldi, A., and Limarino, C. O. (2005). Vallecito Formation (Miocene): the evolution of an eolian system in an Andean foreland basin (northwestern Argentina). *J. South Am. Earth Sci.* 19, 343–357. doi: 10.1016/j.quascirev.2016.03.007

Tripaldi, A., and Zárate, M. A. (2016). A review of late quaternary inland dune systems of South America east of the Andes. *Quat. Int.* 410, 96–110.

Tripaldi, A., Zárate, M. A., Forman, S. L., Badger, T., Doyle, M. E., and Ciccioli, P. (2013). Geologic evidence for a drought episode in the western Pampas (Argentina, South America) during the early-mid 20th century. *Holocene* 23, 1731–1746. doi: 10.1177/0959683613505338

Tsoar, H. (1983). Dynamic processes acting on a longitudinal (seif) sand dune. *Sedimentology* 30, 567–578. doi: 10.1111/j.1365-3091.1983.tb00694.x

Vermeesch, P., Fenton, C. R., Kober, F., Wiggs, G. F. S., Bristow, C. S., and Xu, S. (2010). Sand residence times of one million years in the Namib Sand Sea from cosmogenic nuclides. *Nat. Geosci.* 3, 862–865. doi: 10.1038/ngeo985

von Gosen, W. (1992). Structural evolution of the argentine Precordillera: The San Juan section. *J. Struct. Geol.* 14, 643–667. doi: 10.1016/0191-8141(92)90124-f

Wang, X., Ma, J., Yi, S., Vandenberghe, J., Dai, Y., and Lu, H. (2018). Interaction of fluvial and eolian sedimentation processes, and response to climate change since the last glacial in a semiarid environment along the Yellow River. *Quat. Res.* 570–583. doi: 10.1017/qua.2018.22

Whitehouse, M. J. (2008). Plešovise zircon – a new natural reference material for U-Pb and Hf isotopic microanalysis. *Chem. Geol.* 249, 1–35. doi: 10.1016/j.chemgeo.2007.11.005

Wiedenbeck, M., Alle, P., Corfu, F., Griffin, W. L., Meier, M., Oberli, F. V., et al. (1995). Three natural zircon standards for U—Th—Pb, Lu—Hf, trace element and REE analyses. *Geostand. Newslett.* 19, 1–23. doi: 10.1111/j.1751-908x.1995.tb00147.x

Williams, M. A., and Balling, R. C. Jr. (1996). *Interactions of Desertification and Climate*. London: Hodder Headline, PLC.

Zárate, M. A. (2003). Loess of southern South America. *Quat. Sci. Rev.* 22, 1987–2006. doi: 10.1016/s0277-3791(03)00165-3

Zárate, M. A., and Tripaldi, A. (2012). The aeolian system of central Argentina. *J. Aeol. Res.* 3, 401–417. doi: 10.1016/j.aeolia.2011.08.002

Conflict of Interest: The authors declare that the research was conducted in the absence of any commercial or financial relationships that could be construed as a potential conflict of interest.